SYNTHESES, STRUCTURES, AND PROPERTIES OF NEW MULTI-CHALCOGEN TTF DERIVATIVES, THEIR CHARGE-TRANSFER COMPLEXES AND ION-RADICAL SALTS

1991

HIDEYUKI NAKANO

OSAKA UNIVERSITY

SYNTHESES, STRUCTURES, AND PROPERTIES OF NEW MULTI-CHALCOGEN TTF DERIVATIVES, THEIR CHARGE-TRANSFER COMPLEXES AND ION-RADICAL SALTS

（多数のカルコゲン原子を有する新規ＴＴＦ誘導体およびそれらの電荷移動錯体ならびにイオンラジカル塩の合成、構造および性質）

1991

HIDEYUKI NAKANO

OSAKA UNIVERSITY

Contents

Chapter 3 Crystal Structures and Band Electronic Structures

Introduction

Studies on highly conductive organic charge-transfer complexes and ion-radical salts have been made extensively since the charge-transfer complex of tetrathiafulvalene (TTF) and tetracyanoquinodimethane (TCNQ) was discovered to have high conductivity with metallic behavior down to ca. 60 K in 1973.[1,2]

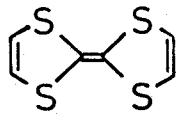

TTF

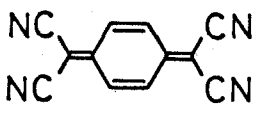

TCNQ

In the crystal of the TTF-TCNQ charge-transfer complex, segregated columns of TTF and TCNQ molecules are formed. Incomplete charge transfer and small on-site Coulomb repulsion energy in the TTF-TCNQ charge-transfer complex cause the high conductivity for this complex. Because of strong intracolumnar interaction and weak intercolumnar interaction, the conductivity of the TTF-TCNQ charge-transfer complex is much higher in the direction along the column than in other directions, and hence TTF-TCNQ is called a quasi-one-dimensional conductor.[3,4]

Although the TTF-TCNQ complex has high conductivity with metallic behavior, the metal-insulator transition occurs at around 60 K.[3,4] This transition is due to a Peierls distortion[5] caused by the one-dimensional instability.

Therefore, the introduction of a two-dimensional character is important to suppress the metal-insulator transition inherent in the one-dimensional system.

The replacement of the sulfur atoms in TTF by selenium atoms whose van der Waals radius is larger than that of the sulfur atom is one approach to have two-dimensional character. Bechgaard and co-workers studied ion-radical salts of tetramethyltetraselenafulvalene (TMTSF).

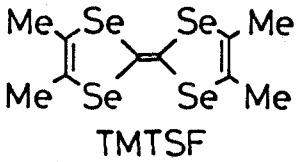

TMTSF

Several $(TMTSF)_2X$ such as $X=NO_3$, PF_6, AsF_6, and BF_4 were prepared and characterized in 1979.[6] These ion-radical salts exhibit metallic behavior with metal-insulator transition at low temperature (ca. 12 K for $X=PF_6$, AsF_6, and NO_3). Shortly thereafter, the studies aimed at suppressing the metal-insulator transition by the application of hydrostatic pressure led to the first observation of superconductivity in the organic conductor, $TMTSF_2PF_6$.[7] After the discovery of superconductivity in $(TMTSF)_2PF_6$, pressure-induced superconductivity of and ambient pressure superconductivity have been found for $(TMTSF)_2X$ [$X=AsF_6$,[8] SbF_6,[9] TaF_6,[10] ReO_4,[11] and FSO_3[12]] and $(TMTSF)_2ClO_4$,[13] respectively. In the crystal of $(TMTSF)_2X$, the columnar structure of TMTSF molecules are formed, and there are not only intracolumnar but also intercolumnar Se-Se contacts shorter than the sum of the van der Waals radii (4.0 Å). That is, the two-dimensional Se-Se network is formed in the crystal.

The introduction of sulfur atoms into the outer sides of TTF is another approach to introduce a two-dimensional character. An example of such a donor is bis(ethylenedithio)-tetrathiafulvalene (BEDT-TTF), and the first superconductor of an ion-radical salt based on BEDT-TTF, $(BEDT\text{-}TTF)_2ReO_4$, was reported in 1983.[14] Since then, a number of superconductors based on BEDT-TTF have been discovered.[14-29]

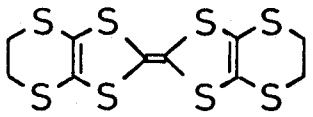

BEDT-TTF

$(BEDT\text{-}TTF)_2Cu[N(CN)_2]Cl$ has the highest superconducting transition temperature[29] (Tc=12.8 K under slight pressure) among the organic superconductors ever known.

In the crystal of β-$(BEDT\text{-}TTF)_2I_3$, the columnar structure of BEDT-TTF molecules are formed and there are many intercolumnar S-S contacts shorter than the van der Waals distance (3.7 Å). Therefore, β-$(BEDT\text{-}TTF)_2I_3$ has a two-dimensional character.[30]

The formation of a columnar structure is not always necessary to introduce a two-dimensional property. In the crystal of κ-$(BEDT\text{-}TTF)_2I_3$, for example, the columnar structure is not formed; however, there are many intermolecular S-S contacts to form two-dimensional S-S networks.[31]

Moreover, bis(ethylenedioxy)tetrathiafulvalene (BEDO-TTF), which is an oxygen containing analogue of BEDT-TTF, has been synthesized[32] and the superconductivity has been reported for $(BEDO\text{-}TTF)_3Cu_2(NCS)_3$.[33]

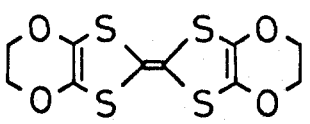

BEDO-TTF

Not only symmetrical donor molecules like TMTSF, BEDT-TTF, and BEDO-TTF, but also unsymmetrical ones have attracted attention since the discovery of the superconductivity in $(DMET)_2Au(CN)_2$[34] (DMET: dimethyl(ethylenedithio)diselenadithiafulvalene) in 1987. Several ion-radical salts based on DMET[34-38] and methylenedithiotetrathiafulvalene (MDT-TTF)[39] have been reported to show superconductivity. They also exhibit a two-dimensional character caused by intermolecular interactions through the chalcogen atoms.

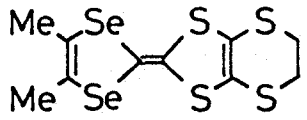

DMET

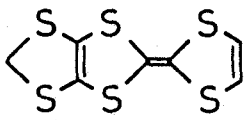

MDT-TTF

The ion-radical salts and charge-transfer complexes of TTF derivatives possessing many chalcogen atoms are expected to exhibit high conductivities and keep the metallic behavior even at low temperature because of the decrease of on-site Coulomb repulsion energy and two-dimensional character due to the intermolecular interaction through the chalcogen atoms.

The aims of this work are to synthesize new symmetrical and unsymmetrical TTF derivatives possessing many chalcogen atoms, their charge-transfer complexes and ion-radical salts, and to investigate the relationship of their structures and electrical properties in order to explore new highly conductive organic materials.

The thesis consists of three chapters. In chapter 1, synthesis of new symmetrical and unsymmetrical TTF derivatives

possessing many chalcogen atoms such as shown below is described, and their oxidation potentials and on-site Coulomb repulsion energy are discussed. In chapter 2, preparation of the charge-transfer complexes and ion-radical salts of the TTF derivatives synthesized in the present study are described, and their electrical conductivities and temperature dependences of conductivity are discussed. Chapter 3 deals with molecular and crystal structures of several neutral donors and ion-radical salts. The band electronic structures of the ion-radical salts are discussed.

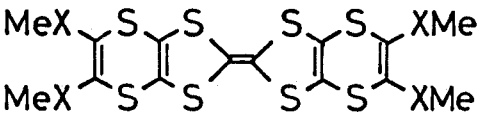

TMTVT: X=S
TMSVT: X=Se

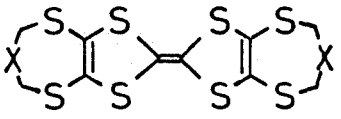

TTT: X=S
OTT: X=O

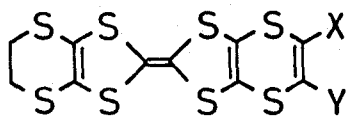

EVT : X=Y=H
EMVT : X=Me, Y=H
EDMVT : X=Y=Me

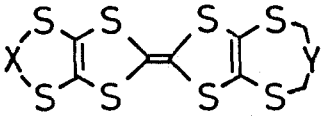

ETTT: X=-CH_2CH_2-, Y=S
TTVT: X=-CH=CH-, Y=S
EOTT: X=-CH_2CH_2-, Y=O

Chapter 1

Synthesis of New Multi-Chalcogen TTF Derivatives

1-1 Introduction

The ion-radical salts of BEDT-TTF have attracted much attention because many of them show superconductivity at low temperature.[14-29] Crystal structures of BEDT-TTF salts exhibit intermolecular S-S contacts shorter than the van der Waals distance to form a two-dimensional S-S network. This two-dimensional crystal structure is considered to be effective for suppressing the metal-insulator transition inherent in the one-dimensional system.[30]

Because of the decrease of the on-site Coulomb repulsion energy and the introduction of the two-dimensional character in the crystal, the ion-radical salts and charge-transfer complexes of TTF derivatives possessing many chalcogen atoms are expected to exhibit high electrical conductivity and keep the metallic behavior down to low temperature. It is of interest to synthesize new TTF derivatives possessing many chalcogen atoms for the development of highly conductive organic materials.

The replacement of the ethylene groups in BEDT-TTF by the other groups is interesting because the change of the crystal

structure caused by the molecular structural change is expected to affect electrical properties of the resulting ion-radical salts and charge-transfer complexes. Thus, analogues of BEDT-TTF possessing methylene or trimethylene groups have been synthesized and the properties of their ion-radical salts have been investigated.[40-48] Not only symmetrical donor molecules but also several unsymmetrical TTF derivatives and their ion-radical salts have been synthesized and characterized.[49-57]

Bis(vinylenedithio)tetrathiafulvalene (VT), which possesses the vinylene group instead of the ethylene group in BEDT-TTF, and its derivatives (DMVT, TMVT) have previously been synthesized,[58-60] and the properties of their ion-radical salts and charge-transfer complexes have been investigated.[61,62]

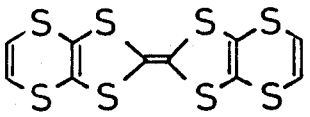

VT

In the present study, the following new symmetrical and unsymmetrical TTF derivatives possessing many chalcogen atoms are synthesized and their oxidation potentials and the on-site Coulomb repulsion energies are discussed.

1) Symmetrical donors possessing twelve chalcogen atoms in a molecule: bis[1,2-bis(methylthio)vinylenedithio]tetrathiafulvalene (TMTVT) and bis[1,2-bis(methylseleno)vinylenedithio]-tetrathiafulvalene (TMSVT).

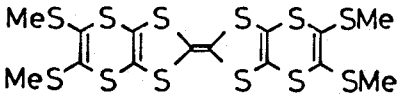

TMTVT

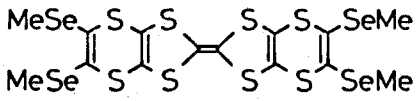

TMSVT

2) Symmetrical donors possessing 2-thia- or 2-oxatrimethylene

groups: bis(2-thiatrimethylenedithio)tetrathiafulvalene (TTT) and bis(2-oxatrimethylenedithio)tetrathiafulvalene (OTT).

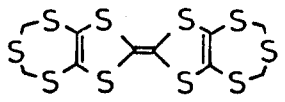

TTT

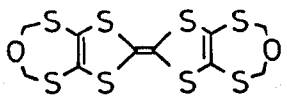

OTT

3) Unsymmetrical donors containing a vinylene group instead of the ethylene group in BEDT-TTF: 4,5-ethylenedithio-4',5'-vinylenedithiotetrathiafulvalene (EVT), 4,5-ethylenedithio-4',5'-(methylvinylenedithio)tetrathiafulvalene (EMVT), and 4,5-ethylenedithio-4',5'-(dimethylvinylenedithio)tetrathiafulvalene (EDMVT).

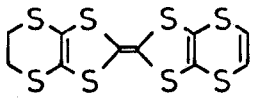

EVT

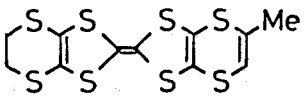

EMVT

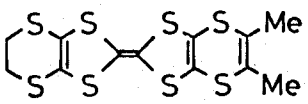

EDMVT

4) Unsymmetrical donor containing a 2-thia-trimethylene group instead of the ethylene group in BEDT-TTF: 4,5-ethylenedithio-4',5'-(2-thia-trimethylenedithio)tetrathiafulvalene (ETTT).

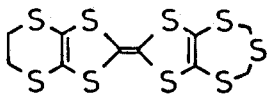

ETTT

5) Unsymmetrical donor containing a 2-thia-trimethylene group instead of the vinylene group in VT: 4,5-(2-thiatrimethylenedithio)-4',5'-vinylenedithiotetrathiafulvalene (TTVT).

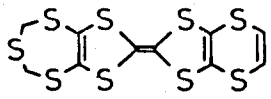

TTVT

6) Unsymmetrical donor containing a 2-oxa-trimethylene group instead of the ethylene group in BEDT-TTF: 4,5-ethylenedithio-4',5'-(2-oxa-trimethylenedithio)tetrathiafulvalene (EOTT).

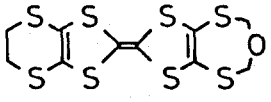

EOTT

1-2 Experimental

1-2-1 Synthesis of TMTVT

i) 4,5-[1,2-Bis(methylthio)vinylenedithio]-1,3-dithiole-2-thione (3a)

A hexane solution of butyllithium (9 mmol) was added to the THF solution (150 ml) of diisopropylamine (0.94 g, 9.3 mmol) at -78°C, and the solution was stirred for 40 min at -78°C under nitrogen atmosphere. 4,5-Vinylenedithio-1,3-dithiole-2-thione[59] (1: 1.00 g, 4.5 mmol) was added to this solution at -78°C. The temperature of the solution was elevated gradually to 0°C, and it was stirred for another 2 h at 0°C to obtain the solution of 2. It was then cooled to -78°C, and sulfur (0.29 g, 9.04 mmol) was added to this solution. The temperature of the solution was elevated gradually to 0°C and the solution was stirred for another 1 h at 0°C to obtain a black solution. The solution was then cooled to -78°C, and methyl iodide (1.4 g, 9.9 mmol) was added with stirring. The temperature of the solution was then allowed to rise to room temperature, and the solution was stirred for another 1 h at this temperature. After evaporating the solvent, the residue was extracted with benzene, washed with water, and the benzene layer dried over Na_2SO_4. The crude product was chromatographed on silica gel using the mixed solvent of chloroform and hexane (1:4) as an eluent. The first pale yellow portion was discarded, and the second orange portion gave a yellow powder of 3a (0.475 g, 33.6%). It was

recrystallized from hexane to obtain yellow needles. Mp 120 - 121°C. MS m/z 314 (M^+). Calcd for $C_7H_6S_7$: C, 26.83; H, 1.98; S, 71.24%. Found C, 26.73; H, 1.92; S, 71.35%. ^{1}H NMR (CS_2) δ = 2.44 (s).

ii) 4,5-[1,2-Bis(methylthio)vinylenedithio]-1,3-dithiol-2-one (4a).

The molecule 3a (300 mg, 0.94 mmol) was dissolved in a mixed solvent of chloroform (30 ml) and acetic acid (30 ml), and mercury(II) acetate (614 mg, 1.93 mmol) was added to this solution. The solution was stirred for 30 min at room temperature, and the pale yellow powder filtered off. The filtrate was washed with water, then with aqueous sodium hydrogencarbonate, and finally with water, and the organic layer was dried over Na_2SO_4. After evaporating the solvent, the residue was chromatographed on silica gel using a mixed solvent of chloroform and hexane (1:1) as eluent, and the second pale yellow portion gave 4a (217 mg, 76.2%). It was recrystallized from hexane to obtain pale yellow needles. Mp 84.0 - 85.0°C. MS m/z 298 (M^+). Calcd for $C_7H_6OS_6$: C, 28.17; H, 2.03; S, 64.44%. Found C, 27.92; H, 2.10; S, 64.42%. ^{1}H NMR (CS_2) δ = 2.43 (s).

iii) Bis[1,2-bis(methylthio)vinylenedithio]tetrathiafulvalene (TMTVT).

The reaction vessel containing 4a (259 mg, 0.868 mmol) was purged with nitrogen gas, and triethyl phosphite (2.5 ml), which

was distilled just before the reaction, was then added. The solution was stirred for a while to obtain a homogeneous solution. It was then heated with stirring, and red powder began to precipitate at around 100°C. It was stirred at 110°C for 2 h. After cooling to room temperature, the red powder was collected, washed with methanol, and dried in vacuum (188 mg, 76.7%). The product was recrystallized from carbon tetrachloride to obtain red needles. Mp 200°C (decomp). MS m/z 564 (M^+). Calcd for $C_{14}H_{12}S_{12}$: C, 29.76; H, 2.14; S, 68.10%. Found C, 29.92; H, 2.09; S, 67.99%. ^{1}H NMR (CS_2) δ = 2.40 (s). UV λ_{max}^{THF} (log ε) 308 nm (4.33), 337 nm (4.30).

1-2-2 Synthesis of TMSVT

i) 4,5-[1,2-Bis(methylseleno)vinylenedithio]-1,3-dithiole-2-thione (3b)

The THF solution of 2 was prepared by the same method for the synthesis of 3a. Well-ground selenium powder (0.711 g, 9.0 mmol) was added to the solution of 2 at -78°C. The temperature of the solution was elevated gradually to 0°C under supersonic wave irradiation using a Bransonic 220 (Yamato Kagaku Co. Ltd). The solution was stirred for another 2.5 h at 0°C to obtain a black solution. No selenium powder could be seen at this stage. The solution was then cooled to -78°C, and methyl iodide (1.4 g, 9.9 mmol) was added with stirring. The temperature of the solution was then allowed to rise to room

temperature, and the solution was stirred for another 1 h at this temperature to obtain a black solution. After evaporating the solvent, the residue was extracted with benzene, washed with water, and the benzene layer dried over Na_2SO_4. The crude product was chromatographed on silica gel using the mixed solvent of chloroform and hexane (1:4) as an eluent. The first pale yellow portion was discarded, and the second orange portion gave a yellow powder of 3b (338 mg, 18.4%). It was recrystallized from the mixed solvent of THF and ethanol to obtain yellow needles. Mp 126 - 127°C. MS m/z 410 (M^+;^{80}Se). Calcd for $C_7H_6S_5Se_2$: C, 20.59; H, 1.48%. Found C, 21.03; H, 1.63%. ^1H NMR (CS_2) δ = 2.37 (s).

ii) 4,5-[1,2-Bis(methylseleno)vinylenedithio]-1,3-dithiol-2-one (4b).

The molecule 3b (200 mg, 0.49 mmol) was dissolved in a mixed solvent of chloroform (40 ml) and acetic acid (40 ml), and mercury(II) acetate (312 mg, 0.98 mmol) was added to this solution. The solution was stirred for 30 min at room temperature, and the pale yellow powder filtered off. The filtrate was washed with water, then with aqueous sodium hydrogencarbonate, and finally with water, and the organic layer was dried over Na_2SO_4. After evaporating the solvent, the residue was chromatographed on silica gel using a mixed solvent of chloroform and hexane (1:1) as eluent, and the first pale yellow portion gave 4b (144 mg, 75%). It was recrystallized from hexane or ethanol to obtain pale yellow needles.

Mp 96.5 - 97.5°C. MS m/z 394 (M^+;^{80}Se). Calcd for $C_7H_6OS_4Se_2$: C, 21.64; H, 1.54%. Found C, 21.64; H, 1.72%. ^{1}H NMR (CS_2) δ = 3.36 (s).

iii) Bis[1,2-bis(methylseleno)vinylenedithio]tetrathiafulvalene (TMSVT).

The reaction vessel containing 4b (204 mg, 0.52 mmol) was purged with nitrogen gas, and triethyl phosphite (2.5 ml), which was distilled just before the reaction, was then added. The solution was stirred for a while to obtain a homogeneous solution. It was then heated with stirring, and red powder began to precipitate at around 100°C. It was stirred at 110°C for 2 h. After cooling to room temperature, the red powder was collected, washed with methanol, and dried in vacuum (0.155 g, 75.1%). The product was recrystallized from carbon tetrachloride to obtain red needles. Mp 185°C (decomp). MS m/z 754 (M^+;^{80}Se). Calcd for $C_{14}H_{12}S_8Se_4$: C, 22.35; H, 1.61%. Found C, 22.24; H, 1.83%. ^{1}H NMR (CS_2) δ = 2.31 (s). UV λ_{max}^{THF} (log ε) 338 nm (4.30), 306 nm (4.37).

1-2-3 Synthesis of TTT

i) 4,5-(2-Thiatrimethylenedithio)-1,3-dithiol-2-one (6a)

4,5-(2-Thiatrimethylenedithio)-1,3-dithiole-2-thione[63] (5a: 1.00 g, 3.9mmol) was dissolved in a mixed solvent of chloroform (300 ml) and acetic acid (100 ml), and mercury(II) acetate (3.58 g, 10.11 mmol) was added to this solution. The solution was

stirred for 30 min at room temperature. The precipitate was filtered off and the filtrate was washed successively with water, aqueous sodium hydrogen carbonate, and water. After the solution was dried over sodium sulfate, the solvent was removed and the crude product was recrystallized from ethanol to give yellow needles (630 mg, 67.3 %). Mp 203 - 205°C. MS m/z 240 (M^+). Calcd for $C_5H_4OS_5$: C, 24.98; H, 1.68; S, 66.69%. Found C, 25.20; H, 1.63; S, 65.84%. ^1H NMR (CS_2) δ = 4.02 (s).

ii) Bis(2-thiatrimethylenedithio)tetrathiafulvalene (TTT).

The triethyl phosphite solution (5 ml) of 6a (481 mg, 2.0 mmol) was stirred at 110°C for 2 h under nitrogen atmosphere. Resulting yellow precipitate was collected, washed with methanol, and dried under reduced pressure. The crude product was recrystallized from o-dichlorobenzene (415 mg, 92.4 %). Mp 252 - 256°C (decomp). MS m/z 448 (M^+). Calcd for $C_{10}H_8S_{10}$: C, 26.76; H, 1.80; S, 71.44%. Found C, 26.98; H, 1.71; S, 70.69%.

1-2-4 Synthesis of OTT

i) 4,5-(2-Oxatrimethylenedithio)-1,3-dithiole-2-thione (5b)

Na (1.47 g, 63.9 mmol) was added to methanol (100 ml) and stirred under nitrogen atmosphere. 4,5-bis(benzoylthio)-1.3-dithiole-2-thione[63] (8.93 g, 22.0 mmol) was added to this solution and the solution was stirred at 5°C for 15 min. After the solution was diluted with methanol (280 ml), the methanol

solution (140 ml) of bis(chloromethyl) ether[64] (12.1 g, 105 mmol) was added and stirred for 2.5 h. The resulting yellow precipitate was collected, washed with water and methanol, and dried under reduced pressure. The crude product was recrystallized from hexane to give yellow needles (4.31 g, 81.6 %). Mp 187 - 188°C. MS m/z 240 (M^+). Calcd for $C_5H_4OS_5$: C, 24.98; H, 1.68; S, 66.69%. Found C, 25.17; H, 1.64; S, 66.98%. ^1H NMR(CS_2) δ = 2.07 (s).

ii) 4,5-(2-Oxatrimethylenedithio)-1,3-dithiol-2-one (6b)

5b (1.12 g, 5.01 mmol) was dissolved in a mixed solvent of chloroform (225 ml) and acetic acid (225 ml), and mercury(II) acetate (3.08 g, 9.66 mmol) was added to this solution. The solution was stirred for 30 min at room temperature. The precipitate was filtered off and the filtrate was washed successively with water, aqueous sodium hydrogen carbonate, and water. After the solution was dried over sodium sulfate, the solvent was removed and the crude product was recrystallized from ethanol to give yellow needles (779 mg; 74.3 %). Mp 163 - 164°C. MS m/z 224 (M^+). Calcd for $C_5H_4O_2S_4$: C, 26.77; H, 1.80; S, 57.17%. Found: C, 26.82; H, 1.77; S, 57.13%. ^1H NMR(CS_2) δ = 2.41 (s).

iii) Bis(2-oxatrimethylenedithio)tetrathiafulvalene (OTT).

The triethyl phosphite solution (3 ml) of 6b (225 mg, 1.0 mmol) was stirred at 110°C for 2 h under nitrogen atmosphere. The resulting yellow precipitate was collected, washed with

methanol, and dried under reduced pressure. The crude product was recrystallized from benzene to give yellow needles (186 mg; 89.0 %). Mp 281 - 283°C (decomp). MS m/z 416 (M^+). Calcd for $C_{10}H_8O_2S_{10}$: C, 28.82; H, 1.94; S, 61.56%. Found C, 28.91; H, 1.87; S, 61.44%. ^{1}H NMR (CS_2) δ = 2.07 (s).
UV λ_{max}^{THF} (log ε) 304 nm (4.52), 335 nm (4.64), 389 nm (3.76).

1-2-5 Synthesis of EVT, EMVT, and EDMVT

i) 4,5-Ethylenedithio-4',5'-vinylenedithiotetrathiafulvalene (EVT).

Triethyl phosphite (20 ml), which had been distilled freshly, was added to a mixture of 4,5-ethylenedithio-1,3-dithiole-2-thione (7: 1.0 g, 4.45 mmol)[63] and 4,5-vinylene-dithio-1,3-dithiol-2-one (8a: 0.92 g, 4.45 mmol).[59] The temperature of the solution was gradually elevated to 110°C with stirring under a nitrogen atmosphere; thereafter, it was stirred for another 2 h at 110°C. After cooling to room temperature, the precipitate was collected, washed with methanol, and dried under a vacuum. The crude product was chromatographed on a silica-gel column, using carbon disulfide as an eluent; the second main fraction gave almost pure EVT (0.75 g, 44%). Recrystallization from benzene gave reddish orange needle crystals. Mp 218°C (decomp). MS m/z 382 (M^+). Calcd for $C_{10}H_6S_8$: C, 31.39; H, 1.58; S, 67.03%. Found C, 31.74; H, 1.57; S, 66.74%. ^{1}H NMR (CS_2) δ = 3.25 (4H, s), 6.47 (2H, s).
UV λ_{max}^{THF} (log ε) 318 nm (4.33), 344 nm (4.24).

ii) 4,5-Ethylenedithio-4',5'-(methylvinylenedithio)tetrathiafulvalene (EMVT) and 4,5-ethylenedithio-4',5'-(dimethylvinylenedithio)tetrathiafulvalene (EDMVT).

EMVT and EDMVT were synthesized under reaction conditions similar as those described for EVT. 4,5-Methylvinylenedithio-1,3-dithiol-2-one[59] (8b) and 4,5-dimethylvinylenedithio-1,3-dithiol-2-one[58] (8c) were used instead of 8a for the synthesis of EMVT and EDMVT, respectively.

EMVT: yield, 61%. orange needles. Mp 210°C (decomp). MS m/z 396 (M^+). Calcd for $C_{11}H_8S_8$: C, 33.30; H, 2.03; S, 64.66%. Found C, 33.40; H, 1.89; S, 64.39%.

^{1}H NMR (CS_2) δ = 2.12 (3H, s), 3.26 (4H, s), 6.02 (1H, s).

UV λ_{max}^{THF} (log ε) 318 nm (4.12), 346 nm (4.02).

EDMVT: yield, 49%. yellow needles. Mp 217°C (decomp). MS m/z 410 (M^+). Calcd for $C_{12}H_{10}S_8$: C, 35.09; H, 2.45; S, 62.45%. Found C, 35.08; H, 2.30; S, 62.35%.

^{1}H NMR (CS_2) δ = 2.03 (6H, s), 3.28 (4H, s).

UV λ_{max}^{THF} (log ε) 318 nm (4.15), 347 nm (4.06).

1-2-6 Synthesis of ETTT, TTVT, and EOTT

i) 4,5-Ethylenedithio-4',5'-(2-thiatrimethylenedithio)tetrathiafulvalene (ETTT).

Triethyl phosphite (16 ml) was added to a mixture of 6a (820 mg; 3.41 mmol) and 7 (765 mg; 3.41 mmol), and the solution was stirred at 110°C for 2 h under nitrogen atmosphere. The resulting precipitate was collected, washed with methanol, and

dried under reduced pressure. The crude product was chromatographed on silica-gel column, using carbon disulfide as an eluent. The orange powder obtained from the second fraction was recrystallized from carbon disulfide to give orange needles (652 mg ; 46 %). Mp 233-235°C (decomp). MS m/z 416 (M^+). Calcd for $C_{10}H_8S_9$: C, 28.93; H, 1.78; S, 68.82%. Found: C, 28.82; H, 1.93; S, 69.25%. ^{1}H NMR(CS_2) δ = 3.28 (4H, s), 3.90 (4H, s). UV λ_{max}^{THF} (log ε) 316 nm (4.20), 342 nm (4.08).

ii) 4,5-(2-Thiatrimethylenedithio)-4',5'-vinylenedithiotetrathiafulvalene (TTVT).

TTVT was synthesized under similar reaction conditions as those for ETTT, using 5a and 8a as starting materials instead of 2 and 3. Recrystallization of crude product from carbon disulfide gave orange needles of TTVT (45%). Mp 225-227°C (decomp). MS m/z 414 (M^+). Calcd for $C_{10}H_6S_9$: C, 28.95; H, 1.33; S, 69.81%. Found: C, 28.96; H, 1.46; S, 69.58%.
^{1}H NMR(CS_2) δ = 3.94 (4H, s), 6.52 (2H, s).
UV λ_{max}^{THF} (log ε) 307 nm (4.14), 339 nm (4.14).

iii) 4,5-Ethylenedithio-4',5'-(2-oxatrimethylenedithio)tetrathiafulvalene (EOTT).

EOTT was also synthesized under similar reaction conditions as those for ETTT, using 6b and 7 as starting materials. Recrystallization of crude product from benzene gave orange needles of EOTT (61.2%). Mp 258 - 260°C (decomp). MS m/z 400 (M^+). Calcd for $C_{10}H_8SO_8$: C, 29.97; H, 2.01; S, 64.02%.

Found C, 30.14; H, 1.98; S, 63.82%.

^{1}H NMR (CS_2) δ = 3.28 (4H, s), 4.72 (4H, s).

UV λ_{max}^{THF} (log ε) 316 nm (4.12), 343 nm (4.03).

1-2-7 Cyclic Voltammetry

Cyclic voltammetry of the donor molecules synthesized was carried out with a Hokuto Denko HA-501 Potentiostat and Hokuto Denko HB-104 Function Generator using platinum plates as the working and counter electrodes and saturated calomel electrode as the reference electrode in acetonitrile containing tetrabutylammonium perchlorate (0.1 M) as the supporting electrolyte.

1-3 Synthesis of TMTVT and TMSVT

The synthetic route of TMTVT and TMSVT is shown in Scheme 1. The molecule 1 was lithiated by lithium diisopropylamide (LDA) to give a solution of 2; thereafter, sulfur or selenium powders were added to this solution. For the selenium insertion reaction, the solution was stirred under supersonic wave irradiation for 2.5 h. Without supersonic wave irradiation, it took 4 - 5 h for the completion of the insertion reaction. The resulting sulfate or selenolate was reacted with methyl iodide to give 4a,b. The conversion of the thiocarbonyl group of 4a,b to a carbonyl group was made by mercury(II)

acetate to give 5a,b. The coupling reaction of 5a,b was made by heating it in neat triethyl phosphite to give TMTVT or TMSVT.

Two other synthetic routes of TMTVT and TMSVT are conceivable. One is a reaction starting with the lithiation of bis(vinylenedithio)tetrathiafulvalene (VT); however, the poor solubility of VT in THF hampered this route. The other is the reaction starting from the lithiation of 4,5-(vinylenedithio)-1,3-dithiol-2-one (8a) followed by the selenium insertion reaction and the subsequent reaction with methyl iodide. However, the carbonyl group of 8a was found to be decomposed after the reaction.

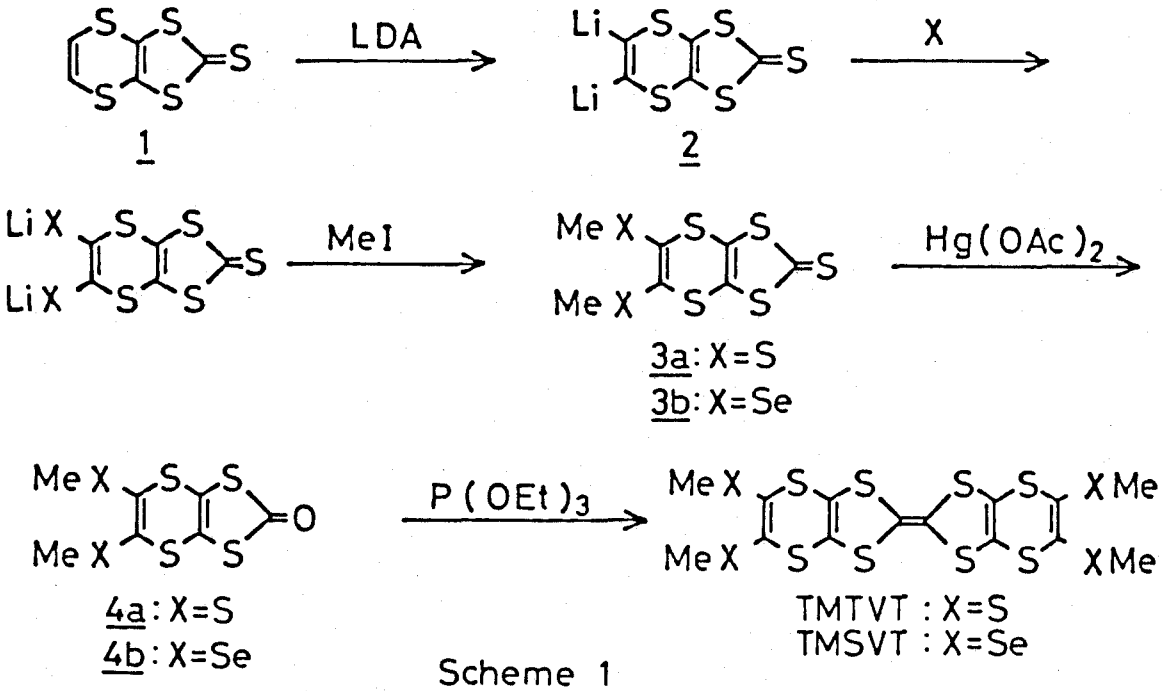

Scheme 1

1-4 Synthesis of TTT and OTT

The synthetic route of TTT and OTT is shown in Scheme 2. The molecule 5 was converted to 6 by the reaction with mercury(II) acetate. The coupling reaction of 6 by triethyl phosphite gave TTT or OTT.

TTT and OTT can be obtained by the coupling reaction of 5; however, both yields of TTT and OTT were lower (51 and 40%, respectively) than those by the two-step reactions (62 and 45% based on 5, respectively).

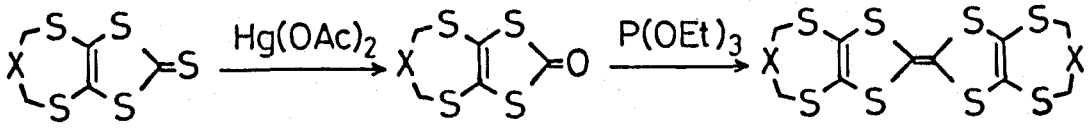

5a: X=S
5b: X=O

6a: X=S
6b: X=O

TTT: X=S
OTT: X=O

Scheme 2

1-5 Synthesis of new unsymmetrical TTF derivatives

The cross-coupling reaction of 7 and 8a, 8b, or 8c gave EVT, EMVT, or EDMVT as the main product. Similarly, ETTT, TTVT, and EOTT can be obtained by the cross-coupling reactions of the corresponding thione and ketone as shown in Scheme 3. In any case, the self-coupling products were obtained as minor products, but the unsymmetrical donor molecule can be easily separated from the self-coupling products by silica-gel column chromatography using carbon disulfide as the eluent.

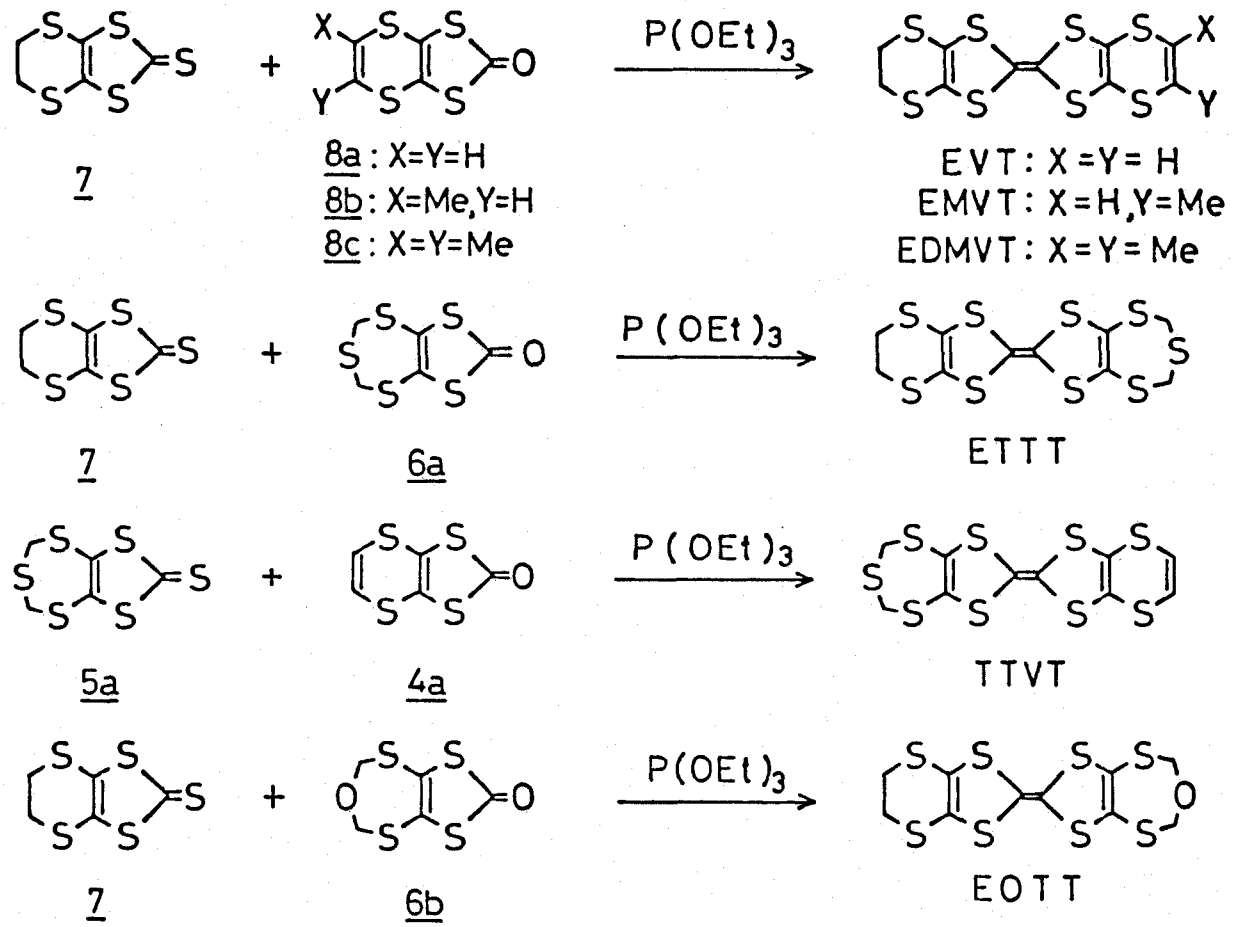

Scheme 3

For the synthesis of the unsymmetrical donors, the cross-coupling reaction of the corresponding thiones were attempted; however, the yields of the cross-coupling products were very low. For example, the coupling reaction of 7 and 6a gave ETTT in a high yield(46%); however, the reaction of 7 and 5a gave BEDT-TTF as a main product and ETTT in a very low yield (5%).

1-6 Redox potentials of the new TTF derivatives

The cyclic voltammetries of the new TTF derivatives synthesized were carried out using tetrabutylammonium perchlorate as an electrolyte and platinum plates as working and counter electrodes in acetonitrile. The first and the second half-wave oxidation potentials (E_1 and E_2) and the differences (ΔE) of E_1 and E_2 are summarized in Table 1 together with those for BEDT-TTF and VT for the sake of comparison. The first oxidation potential of each donor molecule is higher than that of BEDT-TTF, and E_1's of the unsymmetrical donors were found to be intermediate between those of the corresponding symmetrical ones. On the other hand, the difference of E_1 and E_2, which represents the on-site Coulomb repulsion energy, for TTT and OTT are larger than that for BEDT-TTF, but ΔE of VT is smaller than that of BEDT-TTF. The differences ΔE for the unsymmetrical donor molecules are intermediate between those of corresponding symmetrical ones. Thus, the replacement of the ethylene group in BEDT-TTF by the 2-thia- or 2-oxatrimethylene group raises the

Table 1.

The First and the Second Half-wave Oxidation Potentials (E_1 and E_2) of Donor Molecules Together with the Differences (ΔE) of E_1 and E_2

Donor	E_1 V vs. SCE	E_2 V vs. SCE	ΔE ($=E_2-E_1$) V
TMTVT	0.65	0.83	0.18
TMSVT	0.64	0.82	0.18
TTT	0.58	0.84	0.26
OTT	0.59	0.85	0.26
EVT	0.56	0.79	0.23
EMVT	0.56	0.79	0.23
EDMVT	0.55	0.78	0.23
ETTT	0.54	0.79	0.25
TTVT	0.61	0.85	0.24
EOTT	0.54	0.79	0.25
BEDT-TTF	0.50	0.74	0.24
VT	0.63	0.84	0.21

Solvent: CH_3CN ; Supporting Electrolyte: $n\text{-}Bu_4NClO_4$ (0.1M)

first oxidation potential and increases the on-site Coulomb repulsion energy. By contrast, the replacement by the vinylene group raises the first oxidation potential, but decreases the on-site Coulomb repulsion energy. For the donor molecules possessing twelve chalcogen atoms, E_1's of TMTVT and TMSVT are almost equal to that for VT, but ΔE's for TMTVT and TMSVT are smaller than that for VT; therefore, the introduction of the methylthio or methylseleno group into VT decreases the on-site Coulomb repulsion energy.

1-7 Conclusion

New symmetrical and unsymmetrical TTF derivatives possessing many chalcogen atoms have been synthesized, and cyclic voltammetries of these donor molecules carried out. The first half-wave oxidation potentials of these donor molecules are higher than that of BEDT-TTF. The replacement of the ethylene group by the vinylene group or the introduction of the methylthio or methylseleno group decreases the on-site Coulomb repulsion energy, while the replacement by the 2-thia- or 2-oxatrimethylene group increases the on-site Coulomb repulsion energy.

Chapter 2

Synthesis and Electrical Conductivities of Charge-Transfer Complexes and Ion-Radical Salts

2-1 Introduction

Since the donor molecules synthesized in chapter 1 possess many chalcogen atoms in a molecule, their charge-transfer complexes and ion-radical salts are expected to exhibit high electrical conductivities and keep metallic property even at low temperature.

There are several methods to prepare charge-transfer complexes and ion-radical salts. The direct reaction of a donor and an acceptor in solution is the most simple method to prepare charge-transfer complexes. For the preparation of conducting ion-radical salts, electrochemical crystallization is one of the most popular method. Since the ion-radical salts of TMTSF,[6-13] which exhibit superconductivity at low temperature, were prepared by electrochemical crystallization, most of conducting ion-radical salts have been prepared by this method.

In the present study, charge-transfer complexes and ion-radical salts of the new TTF derivatives synthesized in the present study were prepared by the direct reaction method and by

the electrochemical crystallization method, respectively, and their room-temperature conductivities and temperature dependences of conductivities were studied.

2-2 Experimental

2-2-1 Preparation of Charge-Transfer Complexes

The donor and the acceptor were dissolved independently in an appropriate solvent by heating the solution, and then the two solutions mixed. The mixture was allowed to cool to room temperature, and kept at this temperature. The resulting precipitate of a charge-transfer complex was collected and dried under reduced pressure.

2-2-2 Preparation of Ion-Radical Salts

Ion-radical salts were prepared by an electrochemical crystallization method in appropriate solvent under the galvanostatic condition (current: 0.5 - 5.0 μA), using platinum wires as the electrodes and tetrabutylammonium salts as the electrolyte.

2-2-3 Measurements of Electrical Conductivities

For the sample obtained as a single crystal, gold wire was

attached to the crystal by gold paste and the measurement of the conductivity of the sample was carried out by a four- or two-probe method. For the sample obtained as powders, the sample powders were compressed to form pellets by applying a pressure of 30 kg/cm^2. Gold wire was attached to the pellet by gold paste. The conductivity of the pellet was measured by a four-probe method or a van der Pauw's method. Temperature dependences of electrical conductivities of single crystals were measured using a D-type Cryo-mini Refrigerator (Osaka Sanso Co. Ltd.).

2-3 Preparation and Electrical Conductivities of Charge-Transfer Complexes

Charge-transfer complexes of TMTVT, TTT, ETTT, and TTVT were prepared by mixing the solutions of a donor and an acceptor. TCNQ, tetrafluorotetracyanoquinodimethane (F_4TCNQ), 2,3-dichloro-5,6-dicyano-p-benzoquinone (DDQ), and iodine were used as acceptors. The compositions (donor : acceptor) of TTT, ETTT, and TTVT complexes were determined by elemental analysis.

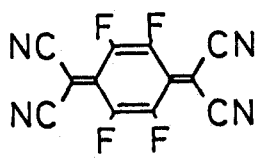

F_4TCNQ

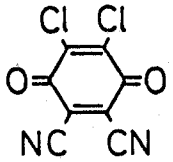

DDQ

Table 2 summarizes the complexes obtained, solvents used for the preparation of the complexes, their appearances, and the results

Table 2.

Preparation, Appearances, and Elemental Analyses of Charge-Transfer Complexes

Complex	Solvent for Preparation[a)]	Appearance	Found (Calcd) %
$TMTVT_xF_4TCNQ$	TCE	dark green needles	b)
$TMTVT_xDDQ$	TCE	black powder	b)
$TMTVT_xI$	TCE	black powder	b)
TTT TCNQ	DCBz	black needles	C,40.74(40.46);H,1.84(1.85); N,8.50(8.58);S,47.32(49.10)
TTT F_4TCNQ	TCE	black powder	C,36.71(36.45);H,1.12(1.11); N,7.46(7.73)
TTT_2I_3	DCBz	black needles	C,18.58(18.79);H,1.24(1.26)
ETTT TCNQ	TCE	black powder	C,42.47(42.55);H,1.88(1.95); N,8.83(9.02);S,46.43(46.48)
ETTT F_4TCNQ	TCE	black powder	C,38.35(38.13);H,1.17(1.16); N,7.92(8.09)
TTVT TCNQ	TCE	black powder	C,42.70(42.69);H,1.62(1.63); N,8.77(9.05);S,46.53(46.63)
$TTVT_5(F_4TCNQ)_3$	TCE	dark green powder	C,35.45(35.59);H,0.99(1.04); N,5.91(5.79)

a) TCE : 1,1,2-trichloroethane, DCBz : o-dichlorobenzene
b) The composition could not be determined because of the unsatisfactory results of elemental analysis.

of elemental analyses. Most of them were found to be 1:1 complexes, but the composition of TTVT-F_4TCNQ complex was 5:3. This is not surprising because complexes having a variety of stoichiometry have been obtained.[62]

The conductivity of TMTVT-F_4TCNQ complex was measured by the two-probe method for single crystals. The conductivities of other complexes obtained were measured for compressed pellet samples because no single crystal with good quality for the conductivity measurement was obtained. Room-temperature conductivities of the complexes are summarized in Table 3. The complexes of TMTVT are not so good conductors ($\sigma = 10^{-6} - 10^{-4}$ S cm^{-1}); however, room-temperature conductivities of the complexes of TTT, ETTT, and TTVT are relatively high for compressed pellet samples ($\sigma = 10^{-2} - 10^{-1}$ S cm^{-1}) except TTVT-F_4TCNQ complex.

The infrared absorption spectra of TTT-, ETTT-, and TTVT-TCNQ complexes were measured by a KBr method in order to estimate the amount of charge transfer. It has been reported that the absorption peak position of the C≡N stretching mode is linearly related to the amount of the charge transfer for the TCNQ complex.[65] The absorption peak position for the neutral TCNQ and completely charge-transferred K TCNQ are 2227 cm^{-1} and 2183 cm^{-1}, respectively. The absorption peak positions and the estimated amounts of charge transfer for the above three complexes are summarized in Table 4. The amount of charge transfer for these complexes were estimated to be similar to that of TTF-TCNQ complex (Z = 0.59), in spite of the fact that

Table 3.

Room-Temperature Conductivities of Charge-Transfer Complexes

Complex	Conductivity / S cm^{-1}	
$TMTVT_xF_4TCNQ$	1.4×10^{-4}	a)
$TMTVT_xDDQ$	8.3×10^{-6}	b)
$TMTVT_xI$	2.7×10^{-5}	b)
TTT TCNQ	8.6×10^{-2}	c)
TTT F_4TCNQ	4.2×10^{-2}	c)
TTT_2I_3	1.2×10^{-2}	c)
ETTT TCNQ	1.2×10^{-1}	c)
ETTT F_4TCNQ	1.3×10^{-5}	c)
TTVT TCNQ	4.5×10^{-1}	b)
$TTVT_5(F_4TCNQ)_3$	1.7×10^{-1}	b)

a) Measured by two-probe method for single crystal.
b) Measured by van der Pauw's method for compressed sample.
c) Measured by four-probe method for compressed sample.

the first oxidation potentials of TTT, ETTT, and TTVT are higher than that of TTF (0.31 V vs. SCE). The amounts of charge-transfer estimated for these complexes are in accord with the high conductivities.

Table 4.
The Absorption Peak Position of the C≡N Stretching Mode and Estimated Amounts of Charge Transfer

Complex	Peak Position cm^{-1}	Amount of Charge Transfer(Z)
TTT TCNQ	2200	0.61
ETTT TCNQ	2197	0.68
TTVT TCNQ	2201	0.59

2-4 Preparation and Electrical Conductivities of Ion-Radical Salts

Ion-radical salts of the donor molecules described in chapter 1 were prepared by electrochemical crystallization using tetrabutylammonium salts as supporting electrolytes. The stoichiometries of these ion-radical salts were determined by elemental analyses or X-ray crystal structure analyses. Table 5 summarizes the ion-radical salts obtained, solvents used for the preparation, their appearances, and the results of elemental analyses.

Room-temperature conductivities and activation energies

Table 5.
Preparation, Appearances, and Elemental Analyses of Ion-radical Salts

Salt	Solvent for Preparation[a)]	Appearance of Salt	Found (Calcd) %
$TMTVT_xPF_6$	TCE	black needles	b)
OTT_2AsF_6	THF	black plates	C,23.67(23.50);H,1.56(1.58)
OTT_2AuCl_2	THF	black needles	C,22.00(21.81);H,1.54(1.46)
EVT_2PF_6	THF	black needles	c)
EVT_2AsF_6	PhCl	black needles	c)
EVT_2IBr_2	$PhNO_2$	black needles	C,22.22(22.83);H,1.12(1.15)
EVT_2AuBr_2	$PhNO_2$	black plates	C,21.44(21.41);H,1.13(1.08)
EVT_2AuCl_2	THF	black needles	C,23.15(23.25);H,1.19(1.17)
EVT_2ReO_4	TCE	black needles	C,23.69(23.65);H,1.22(1.19)
$TTVT_xI_3$	TCE	black powder	b)
$ETTT_2PF_6$	PhCl	black plates	C,24.88(24.55);H,1.69(1.65)
$ETTT_2AsF_6$	PhCl	black plates	C,23.54(23.49);H,1.56(1.58)
$ETTT_2IBr_2$	THF	black powder	C,21.96(21.44);H,1.46(1.44)
$ETTT_xAuBr_2$	DCBz	black powder	b)
$ETTT_xAuI_2$	DCBz	black needles	b)
$ETTT_2AuCl_2$	DCBz	black needles	C,21.88(21.81);H,1.50(1.46)
$EOTT_2PF_6$	THF	black plates	C,25.36(25.38);H,1.67(1.70)
$EOTT_2AsF_6$	THF	black plates	C,24.26(24.26);H,1.59(1.63)
$EOTT_2SbF_6$	THF	black plates	C,23.45(23.16);H,1.58(1.56)
$EOTT_xBr_3$	THF	black needles	b)
$EOTT_2IBr_2$	THF	black needles	C,22.04(22.08);H,1.32(1.48)
$EOTT_2I_3$	PhCl	black needles	C,20.40(20.32);H,1.30(1.36)
$EOTT_2AuBr_2$	THF	black needles	C,20.94(20.74);H,1.50(1.39)
$EOTT_2AuI_2$	THF	black needles	c)

a) TCE : 1,1,2-trichloroethane, DCBz : o-dichlorobenzene
b) The composition could not be determined because of the unsatisfactory results of elemental analysis.
c) The composition was determined by X-ray crystal structure analysis (see chapter 3).

Table 6.
Room-Temperature Conductivities of Ion-radical Salts Together with Activation Energies (Ea) for Electrical Conduction

Salt	Conductivity[a] / S cm^{-1}		Ea / eV
$TMTVT_xPF_6$	2.5×10^{-4}	b)	
OTT_2AsF_6	0.026		0.11
OTT_2AuCl_2	0.19		0.08
EVT_2PF_6	0.76		0.14
EVT_2AsF_6	0.17		0.11
EVT_2IBr_2	18		0.04
EVT_2AuBr_2	51		0.05
EVT_2AuCl_2	17		0.07
EVT_2ReO_4	50		metallic
$TTVT_xI_3$	27	c,d)	0.04
$ETTT_2PF_6$	0.28		0.07
$ETTT_2AsF_6$	2.0		0.06
$ETTT_2IBr_2$	1.2	d)	0.07
$ETTT_xAuBr_2$	0.21	d)	
$ETTT_xAuI_2$	28		metallic
$ETTT_2AuCl_2$	1.9		0.06
$EOTT_2PF_6$	0.29		0.04
$EOTT_2AsF_6$	0.52		0.06
$EOTT_2SbF_6$	0.74		0.11
$EOTT_xBr_3$	40		metallic
$EOTT_2IBr_2$	55		metallic
$EOTT_2I_3$	4.0		0.19
$EOTT_2AuBr_2$	17		metallic
$EOTT_2AuI_2$	170		metallic

a) Measured by four-probe method.
b) Measured by two-probe method.
c) Measured by van der Pauw's method.
d) Measured for compressed sample.

for electrical conduction of the ion-radical salts are summarized in Table 6. The ion-radical salts obtained show high conductivities in the range from 10^{-2} to 10^{2} S cm^{-1} except for $TMTVT_xPF_6$ (2.5×10^{-4} S cm^{-1}). Many of them showed semiconducting behavior but their activation energies for electrical conduction are very small (ca. 0.1 eV).

Several ion-radical salts exhibited metallic behavior. Among them, $ETTT_2AuI_2$, $EOTT_xBr_3$, and $EOTT_2AuBr_2$ showed metal-insulator transition at 250, 251, and 210 K, respectively. EVT_2ReO_4, $EOTT_2IBr_2$, and $EOTT_2AuI_2$ kept the metallic property down to 4.2 K (Fig. 1).

2-5 Conclusion

Charge-transfer complexes and ion-radical salts of the donor molecules synthesized in chapter 1 have been prepared, and their electrical conductivities examined. The conductivities of TTT-, ETTT-, and TTVT-TCNQ complexes are fairly high (σ = 10^{-1}-10^{-2} S cm^{-1}). The high conductivities of the TCNQ complexes of the three donors are in accord with the amount of charge transfer as estimated from the infrared absorption spectroscopy. A variety of ion-radical salts have been obtained by the electrochemical crystallization. Some of them show metallic behavior in electrical conduction. Among them, EVT_2ReO_4, $EOTT_2IBr_2$, and $EOTT_2AuI_2$ kept metallic property down to 4.2 K.

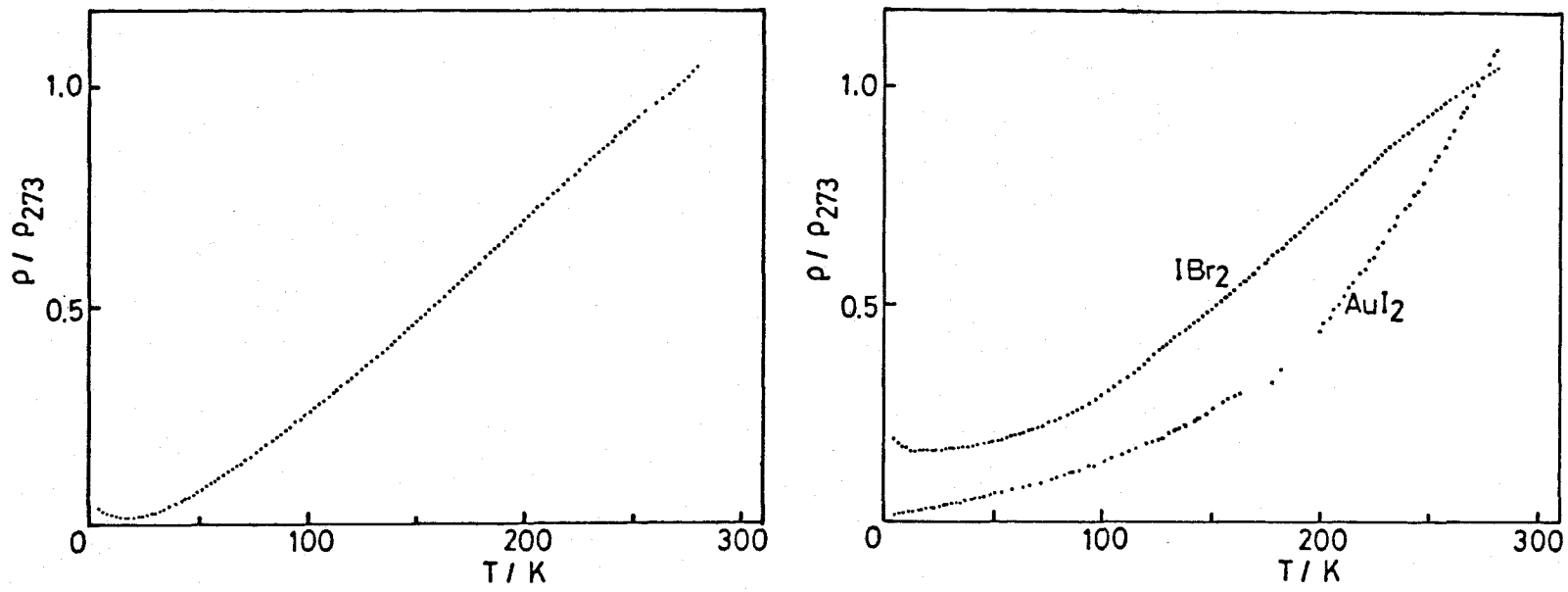

Fig. 1. Temperature dependences of the resistivities of (a) EVT_2ReO_4, (b) $EOTT_2IBr_2$ and $EOTT_2AuI_2$ (normalized to those at 273K).

Chapter 3

Crystal Structures and Band Electronic Structures

3-1 Introduction

Crystal structure analysis is important to examine the relationship between the structure and the property of organic conductors. Crystal structures of a variety of ion-radical salts which exhibit superconductivity at low temperature have been determined. It is shown that two-dimensional chalcogen-chalcogen networks are formed in these crystals. It has been suggested that the formation of two-dimensional chalcogen-chalcogen networks plays an important role in suppressing the metal-insulator transition inherent in the one-dimensional system.[30]

In the present study, X-ray structure analyses were carried out for neutral donor molecules, TMTVT and EVT, and several ion-radical salts of EVT and EOTT. In addition, the band electronic calculations based on a tight binding method were made for the ion-radical salts, using molecular orbitals obtained by an extended Hückel method.[66] This calculation is useful for discussing electrical properties of organic conductors. The results of the band electronic calculation for

the ion-radical salts of EVT were compared with those of the ion-radical salts of corresponding symmetrical donors, BEDT-TTF and VT. The result of the calculation for $EOTT_2IBr_2$ is in accord with the fact that this ion-radical salt exhibits metallic behavior down to low temperature (4.2 K).

3-2 Experimental

3-2-1 Determination of Molecular and Crystal Structures of TMTVT

$C_{14}H_{12}S_{12}$, M = 565.04, monoclinic, space group $P2_1/n$, a = 7.939(1), b = 28.302(2), c = 5.067(1) Å, β = 95.74(1)°, V = 1132.8(2) $Å^3$, D_c = 1.657 g cm^{-3} for Z = 2. The crystal used had a needle shape with 0.04 x 0.16 x 0.46 mm^3. Reflection intensities were measured by the θ-2θ scan technique up to 2θ = 120° on a Rigaku rotating anode four-circle diffractometer using nickel-filtered Cu K_α radiation (λ = 1.542 Å). The scan rate (θ) was 4° min^{-1} and the scan width Δθ = (1.4 + 0.15 tanθ)°. Backgrounds were counted for 3 s at both ends of each scan. No significant intensity decay of the standard reflections, which were measured after every 100 reflections, was detected. Of the 1997 reflections measured, 1564 were observed ($|F_o| > 2\sigma(F_o)$). The usual Lorentz and polarization corrections were applied, but no absorption correction was made [μ(Cu K_α) = 102.8 cm^{-1}].

The structure was solved by a direct method (MULTAN 78)[67],

Table 7.

Atomic Parameters of Nonhydrogen Atoms of TMTVT with Equivalent Isotropic Temperature Factors[70] and Their Estimated Standard Deviations in Parentheses

Atom	X	Y	Z	$B_{eq}/Å^2$
C(1)	0.9558(5)	0.0132(1)	0.0785(9)	3.77
C(2)	0.7200(5)	0.0521(1)	0.320(1)	3.84
C(3)	0.8654(5)	0.0710(1)	0.429(1)	4.09
C(4)	0.5610(6)	0.1337(2)	0.388(1)	4.42
C(5)	0.7065(6)	0.1530(2)	0.494(1)	4.30
C(6)	0.3231(9)	0.1415(3)	-0.051(1)	7.01
C(7)	0.9400(8)	0.2188(3)	0.350(2)	7.6
S(1)	0.7329(1)	0.01139(4)	0.0630(3)	4.14
S(2)	1.0537(1)	0.05421(4)	0.3074(3)	4.31
S(3)	0.5240(1)	0.07249(4)	0.3995(3)	4.29
S(4)	0.8665(2)	0.11692(5)	0.6626(3)	4.61
S(5)	0.3871(2)	0.16848(6)	0.2647(4)	5.99
S(6)	0.7490(2)	0.21363(5)	0.5121(4)	6.10

Table 8.

Thermal Parameters of Nonhydrogen Atoms of TMTVT in the Form of $\exp(-(B(11)*h^2+B(22)*k^2+B(33)*l^2+B(12)*h*k+B(13)*h*l+B(23)*k*l))$ and Their Estimated Standard Deviations in Parentheses

Atom	B(11)	B(22)	B(33)	B(12)	B(13)	B(23)
C(1)	0.0082(6)	0.00123(6)	0.052(2)	0.0009(3)	0.003(2)	0.0023(6)
C(2)	0.0081(6)	0.00117(6)	0.056(3)	0.0007(3)	0.001(2)	0.0006(6)
C(3)	0.0106(7)	0.00122(6)	0.055(3)	0.0015(3)	-0.000(3)	0.0012(6)
C(4)	0.0122(8)	0.00168(7)	0.047(2)	0.0017(4)	0.004(2)	-0.0004(6)
C(5)	0.0107(7)	0.00133(6)	0.059(3)	0.0010(4)	0.005(2)	0.0005(6)
C(6)	0.022(1)	0.0028(1)	0.062(3)	0.0004(7)	-0.005(4)	0.002(1)
C(7)	0.023(1)	0.0021(1)	0.110(5)	-0.0024(6)	0.041(5)	-0.000(1)
S(1)	0.0080(2)	0.00136(2)	0.0589(6)	0.00011(7)	0.0019(5)	-0.0024(2)
S(2)	0.0074(2)	0.00144(2)	0.0628(6)	0.00039(7)	0.0002(5)	-0.0012(2)
S(3)	0.0082(2)	0.00136(2)	0.0644(6)	0.00007(7)	0.0090(5)	-0.0011(2)
S(4)	0.0129(2)	0.00151(2)	0.0551(6)	0.00060(9)	-0.0069(6)	-0.0028(2)
S(5)	0.0171(3)	0.00198(3)	0.0706(8)	0.0055(1)	-0.0047(7)	-0.0013(2)
S(6)	0.0184(3)	0.00116(2)	0.102(1)	-0.00011(9)	0.0294(9)	-0.0042(2)

and was refined anisotropically by a block-diagonal least-squares procedure (HBLS V).[68] The function minimized was $\Sigma w(\Delta F)^2$. The weighting function used in the final stage of the refinement was $w = [\sigma^2(F_o)-0.0826|F_o|+ 0.0166|F_o|^2]^{-1}$. The hydrogen atoms could not be found on a D-map, which is probably due to either the rotation or the large amplitude of vibration of the methyl group. Therefore, hydrogen atoms were not included in the final refinement. Atomic scattering factors were taken from those of International Tables for X-Ray Crystallography.[69] The final R index was 0.091. The atomic coordinates and equivalent isotropic temperature factors[70] are given in Table 7, and anisotropic temperature factors in Table 8.

3-2-2 Determination of Molecular and Crystal Structures of EVT

$C_{10}H_6S_8$, M = 382.68, monoclinic, space group $P2_1/n$, a = 6.563(1), b = 13.507(8), c = 15.866(8) Å, β = 93.47(2)°, V = 1404(1) Å^3, D_c = 1.80 g cm^{-3} for Z = 4. The crystal used had a needle shape with approximate dimensions of 0.19 x 0.60 x 0.18 mm^3. The reflection intensities were measured by the θ-2θ scan technique up to 2θ = 55° on a Rigaku AFC-4 four-circle diffractometer, using Mo K_α radiation (λ = 0.7107 Å). The scan rate (θ) was 4° min^{-1}, and the scan width, $\Delta\theta$ = (1.20 + 0.5 tanθ)°. Backgrounds were counted for 3 s at both ends of a scan. No significant intensity decay of the standard reflections, which were measured after every 100 reflections,

Table 9.

Atomic Parameters of Nonhydrogen Atoms of EVT with Equivalent Isotropic Temperature Factors[70] and Their Estimated Standard Deviations in Parentheses

Atom	x	y	z	$B_{eq}/Å^2$
C(1)	0.1049(8)	0.0455(5)	0.3656(4)	2.4
C(2)	0.0823(9)	-0.0236(5)	0.2143(4)	3.2
C(3)	0.278(1)	-0.0347(6)	0.2432(4)	3.6
C(4)	0.168(1)	-0.1268(7)	0.0728(5)	5.7
C(5)	0.375(1)	-0.0816(8)	0.0835(6)	6.1
C(6)	0.0677(8)	0.0970(5)	0.4362(4)	2.5
C(7)	-0.0831(9)	0.2199(5)	0.5374(4)	2.9
C(8)	0.1120(9)	0.2114(5)	0.5652(4)	2.6
C(9)	-0.175(1)	0.2847(6)	0.6917(5)	4.6
C(10)	0.024(1)	0.2773(6)	0.7200(5)	4.4
S(1)	-0.0877(3)	0.0184(1)	0.2877(1)	3.2
S(2)	0.3430(3)	-0.0045(1)	0.3478(1)	3.3
S(3)	-0.0278(3)	-0.0524(2)	0.1143(1)	4.3
S(4)	0.4806(3)	-0.0800(3)	0.1877(1)	6.3
S(5)	-0.1765(3)	0.1414(1)	0.4571(1)	3.0
S(6)	0.2558(3)	0.1195(1)	0.5175(9)	2.9
S(7)	-0.2554(3)	0.2992(1)	0.5839(1)	3.9
S(8)	0.2262(3)	0.2771(1)	0.6501(1)	3.9

Table 10.

Thermal Parameters of Nonhydrogen Atoms of EVT in the Form of $\exp(-(B(11)*h^2+B(22)*k^2+B(33)*l^2+B(12)*h*k+B(13)*h*l+B(23)*k*l))$ and Their Estimated Standard Deviations in Parentheses

Atom	B(11)	B(22)	B(33)	B(12)	B(13)	B(23)
C(1)	0.014(1)	0.0042(4)	0.0019(2)	0.002(1)	-0.0000(8)	-0.0007(5)
C(2)	0.016(1)	0.0062(5)	0.0024(3)	-0.002(1)	0.0008(9)	-0.0008(5)
C(3)	0.019(2)	0.0073(5)	0.0025(3)	0.000(1)	0.002(1)	-0.0018(6)
C(4)	0.025(2)	0.0109(8)	0.0048(4)	0.009(2)	-0.005(1)	-0.0073(9)
C(5)	0.027(3)	0.0126(9)	0.0045(4)	0.003(3)	0.003(2)	-0.006(1)
C(6)	0.013(1)	0.0039(4)	0.0026(3)	-0.003(1)	0.0010(8)	0.0004(5)
C(7)	0.020(2)	0.0032(4)	0.0030(3)	0.002(1)	0.002(1)	-0.0004(5)
C(8)	0.016(1)	0.0041(4)	0.0022(3)	-0.001(1)	0.0019(9)	-0.0011(5)
C(9)	0.032(3)	0.0060(5)	0.0039(4)	-0.003(2)	0.005(1)	-0.0023(7)
C(10)	0.028(2)	0.0072(5)	0.0032(3)	-0.003(2)	0.006(1)	-0.0023(7)
S(1)	0.0136(4)	0.0068(1)	0.00233(6)	0.0033(3)	-0.0007(3)	-0.0020(1)
S(2)	0.0148(4)	0.0068(1)	0.00248(6)	0.0039(4)	-0.0008(3)	-0.0013(1)
S(3)	0.0181(4)	0.0102(2)	0.00249(7)	0.0014(4)	-0.0003(3)	-0.0035(2)
S(4)	0.0159(4)	0.0165(3)	0.0045(1)	0.0013(6)	0.0035(4)	-0.0086(3)
S(5)	0.0137(3)	0.0052(1)	0.00295(6)	0.0017(3)	-0.0006(3)	-0.0015(1)
S(6)	0.0151(4)	0.00473(9)	0.00268(6)	0.0015(3)	-0.0014(3)	-0.0013(1)
S(7)	0.0223(5)	0.0052(1)	0.00417(8)	0.0055(4)	0.0030(3)	-0.0019(2)
S(8)	0.0217(4)	0.0065(1)	0.00324(7)	-0.0066(4)	0.0018(3)	-0.0037(2)

was detected. Of the 3513 reflections measured, the number of reflections observed was 2517 ($|F_o| > 2\sigma(F_o)$). The usual Lorentz and polarization corrections were applied, but no absorption correction was made [μ(Mo K_α) = 11.9 cm^{-1}].

The structure was solved by the direct method (MULTAN 78)[67] and was refined anisotropically by a block-diagonal least-squares procedure (HBLS V).[68] The hydrogen atoms could not be found on a D-map, probably because of their large thermal motion. Therefore, the hydrogen atoms were omitted in the final refinement. The function minimized was $\Sigma w(\Delta F)^2$. The weighting function used in the final stage of the refinement was $w = [\sigma^2(F_o) + 0.0654|F_o| + 0.0005|F_o|^2]^{-1}$. The atomic scattering factors were taken from those of the International Tables for X-Ray Crystallography.[69] The final R index was 0.070. The atomic coordinates of non-hydrogen atoms with equivalent isotropic temperature factors[70] are given in Table 9, and anisotropic temperature factors in Table 10.

3-2-3 Determination of Molecular and Crystal Structures of EVT_2PF_6 and EVT_2AsF_6

EVT_2PF_6: $(C_{10}H_6S_8)_2PF_6$, M = 910.33, triclinic, space group $P\bar{1}$, a = 6.47(2), b = 7.80(3), c = 15.81(5) Å, α = 94.8(8), β = 80.2(3), γ = 100.2(6)°, V = 772(5) $Å^3$, Z = 1, D_c = 1.96 g cm^{-3}, μ(Mo K_α) = 11.8 cm^{-1}; EVT_2AsF_6: $(C_{10}H_6S_8)_2AsF_6$, M = 954.28, triclinic, $P\bar{1}$, a = 6.494(1), b = 7.760(2), c = 16.039(4) Å, α = 94.97(2), β = 98.63(1), γ = 79.58(2)°, V = 784.5(3) $Å^3$, Z = 1,

D_c = 2.02 g cm^{-3}, μ(Mo K_α) = 21.6 cm^{-1}. The crystals were needle shaped with approximate dimensions of 0.78 x 0.21 x 0.08 mm^3 for EVT_2PF_6 and 0.53 x 0.28 x 0.10 mm^3 for EVT_2AsF_6. X-ray diffraction data were collected by the θ-2θ scan technique up to 2θ = 47° and 50° for EVT_2PF_6 and EVT_2AsF_6, respectively, on a Rigaku AFC-4 four-circle diffractometer, using graphite monochromatized Mo K_α radiation (λ = 0.7107 Å). The scan rates (θ) were 2° min^{-1} for EVT_2PF_6 and 4° min^{-1} for EVT_2AsF_6, and the scan widths $\Delta\theta$ = (1.2 + 0.5 tanθ)° for EVT_2PF_6 and $\Delta\theta$ = (1.0 + 0.5 tanθ)° for EVT_2AsF_6. Backgrounds were counted for 5 s at both ends of each scan. No significant intensity decay of three standard reflections, which were measured after every 100 reflections, were detected for either crystal. For EVT_2PF_6, of the 2523 reflections measured, 1778 were observed ($|F_o| > 2\sigma(F_o)$). For EVT_2AsF_6, of the 2990 reflections measured, 2565 were observed ($|F_o| > 2\sigma(F_o)$). The data were corrected for both Lorentz and polarization factors, but not for absorption.

The structures were solved by a direct method (MULTAN 78),[67] and were refined anisotropically by a block-diagonal least-squares procedure (HBLS V) for nonhydrogen atoms.[68] Not all of the hydrogen atoms could be reasonably refined. Thus, they were relocated at the calculated positions with the isotropic temperature factors set equal to those of bonded carbon atoms. They were included in the calculations but were not refined. The minimized function was $\Sigma w(\Delta F)^2$. The weighting functions used in the final stage of the refinements were $w = [\sigma^2(F_o) - 0.0045|F_o| + 0.0149|F_o|^2]^{-1}$ for EVT_2PF_6 and

Table 11-a.

Atomic Parameters of Nonhydrogen Atoms of EVT_2PF_6 with Equivalent Isotropic Temperature Factors[70] and Their Estimated Standard Deviations in Parentheses

Atom	x	y	z	$B_{eq}/Å^2$
C(1)	0.492(2)	0.284(2)	0.5180(8)	2.8
C(2)	0.532(3)	0.172(2)	0.3609(8)	2.9
C(3)	0.324(3)	0.151(2)	0.3864(9)	2.9
C(4)	0.453(3)	0.092(3)	0.1958(9)	4.4
C(5)	0.251(3)	-0.005(3)	0.233(1)	5.6
C(6)	0.525(2)	0.338(1)	0.6009(8)	2.2
C(7)	0.683(2)	0.461(2)	0.7356(7)	2.1
C(8)	0.476(2)	0.429(2)	0.7616(8)	2.9
C(9)	0.749(3)	0.399(2)	0.8942(8)	3.2
C(10)	0.537(3)	0.361(2)	0.9149(8)	3.5
S(1)	0.6982(5)	0.2619(5)	0.4374(3)	3.0
S(2)	0.2399(6)	0.2125(5)	0.4932(3)	3.3
S(3)	0.6658(6)	0.1268(6)	0.2597(3)	4.0
S(4)	0.1193(6)	0.0715(6)	0.3288(3)	3.6
S(5)	0.7766(6)	0.4044(5)	0.6299(2)	2.8
S(6)	0.3166(5)	0.3484(5)	0.6836(3)	2.9
S(7)	0.8696(6)	0.5257(5)	0.8068(3)	3.4
S(8)	0.3599(6)	0.4554(5)	0.8664(3)	3.2
P	0. (0)	0. (0)	0. (0)	2.8
F(1)	0.014(3)	0.201(1)	0.0221(8)	7.8
F(2)	-0.231(1)	-0.012(2)	-0.0213(7)	6.1
F(3)	0.091(2)	0.042(1)	-0.0957(6)	5.9

Table 11-b.

Calculated Positional Parameters and Assumed Thermal Parameters of Hydrogen Atoms of EVT_2PF_6

Atom	X	Y	Z	B[a)]
H(4a)	0.1461	-0.0134	0.1856	5.6
H(4b)	0.2779	-0.1345	0.2418	5.6
H(5a)	0.5080	0.0230	0.1363	4.4
H(5b)	0.4260	0.2184	0.1818	4.4
H(9)	0.4709	0.2684	0.9635	3.5
H(10)	0.8482	0.3513	0.9322	3.2

a) Thermal Parameters in the Form of $\exp(-B^*(\sin\theta/\lambda)^2)$

Table 12.

Thermal Parameters of Nonhydrogen Atoms of EVT_2PF_6 in the Form of $\exp(-(B(11)*h^2+B(22)*k^2+B(33)*l^2+B(12)*h*k+B(13)*h*l+B(23)*k*l))$ and Their Estimated Standard Deviations in Parentheses

Atom	B(11)	B(22)	B(33)	B(12)	B(13)	B(23)
C(1)	0.012(3)	0.018(3)	0.0027(6)	0.009(5)	-0.003(3)	-0.005(2)
C(2)	0.022(4)	0.007(3)	0.0034(6)	0.003(5)	-0.006(3)	-0.005(2)
C(3)	0.023(4)	0.013(3)	0.0026(6)	0.009(5)	-0.007(3)	-0.002(2)
C(4)	0.023(5)	0.039(5)	0.0032(7)	0.010(8)	-0.004(3)	-0.010(3)
C(5)	0.026(5)	0.023(4)	0.0035(7)	0.003(7)	-0.011(3)	-0.008(3)
C(6)	0.017(4)	0.003(2)	0.0029(6)	-0.004(4)	-0.001(3)	-0.001(2)
C(7)	0.019(4)	0.010(3)	0.0030(6)	-0.001(5)	-0.006(3)	-0.004(2)
C(8)	0.012(3)	0.013(3)	0.0019(5)	0.005(5)	-0.006(2)	-0.002(2)
C(9)	0.033(5)	0.015(3)	0.0020(6)	0.006(6)	-0.008(3)	-0.002(2)
C(10)	0.022(4)	0.018(3)	0.0021(6)	0.008(6)	-0.005(3)	0.000(2)
S(1)	0.0158(9)	0.0204(8)	0.0025(2)	-0.001(2)	-0.0027(6)	-0.0038(6)
S(2)	0.0159(9)	0.0166(7)	0.0026(2)	0.003(2)	-0.0034(6)	-0.0047(5)
S(3)	0.018(1)	0.0222(9)	0.0031(2)	-0.006(2)	-0.0047(6)	-0.0050(6)
S(4)	0.018(1)	0.028(1)	0.0024(2)	0.009(2)	-0.0031(6)	-0.0064(6)
S(5)	0.0171(9)	0.0142(7)	0.0026(2)	-0.001(2)	-0.0031(6)	-0.0035(5)
S(6)	0.0176(9)	0.0148(7)	0.0022(2)	0.001(2)	-0.0036(6)	-0.0032(5)
S(7)	0.021(1)	0.0153(7)	0.0026(2)	0.006(2)	-0.0017(6)	-0.0024(5)
S(8)	0.0194(9)	0.0175(8)	0.0030(2)	-0.005(2)	-0.0061(6)	-0.0017(6)
P	0.020(2)	0.0110(9)	0.0026(2)	-0.005(2)	-0.0063(9)	0.0001(7)
F(1)	0.073(6)	0.013(2)	0.0087(8)	0.006(5)	-0.011(4)	-0.006(2)
F(2)	0.020(3)	0.041(3)	0.0063(6)	-0.006(5)	-0.011(2)	0.005(2)
F(3)	0.034(3)	0.036(3)	0.0034(4)	-0.014(5)	-0.005(2)	0.001(2)

Table 13-a.

Atomic Parameters of Nonhydrogen Atoms of EVT_2AsF_6 with Equivalent Isotropic Temperature Factors[70] and Their Estimated Standard Deviations in Parentheses

Atom	x	y	z	$B_{eq}/Å^2$
C(1)	0.5103(7)	0.2812(6)	0.5211(3)	3.0
C(2)	0.6771(8)	0.1498(6)	0.3899(3)	3.0
C(3)	0.4687(8)	0.1710(6)	0.3641(3)	3.1
C(4)	0.753(1)	-0.010(1)	0.2363(4)	6.6
C(5)	0.5489(9)	0.0923(8)	0.2004(4)	4.2
C(6)	0.4759(7)	0.3398(6)	0.6010(3)	2.8
C(7)	0.5221(7)	0.4333(6)	0.7591(3)	2.8
C(8)	0.3148(7)	0.4601(6)	0.7351(3)	2.8
C(9)	0.4610(9)	0.3674(7)	0.9131(3)	3.7
C(10)	0.2506(9)	0.4059(8)	0.8913(4)	4.1
S(1)	0.7610(2)	0.2141(2)	0.4940(1)	3.6
S(2)	0.3041(2)	0.2623(2)	0.4391(1)	3.4
S(3)	0.8839(2)	0.0699(3)	0.3313(1)	4.2
S(4)	0.3384(3)	0.1227(3)	0.2639(1)	4.3
S(5)	0.6831(2)	0.3508(2)	0.6821(1)	3.3
S(6)	0.2233(2)	0.4054(2)	0.6298(1)	3.1
S(7)	0.6390(2)	0.4593(2)	0.8640(1)	3.7
S(8)	0.1280(2)	0.5299(2)	0.8049(1)	3.8
As	0. (0)	0. (0)	0. (0)	3.2
F(1)	-0.008(1)	0.2184(5)	0.0208(3)	8.7
F(2)	0.2481(6)	-0.0220(7)	-0.0259(3)	7.6
F(3)	-0.1007(6)	0.0351(6)	-0.1027(2)	6.5

Table 13-b.

Calculated Positional Parameters and Assumed Thermal Parameters of Hydrogen Atoms of EVT_2AsF_6

Atom	X	Y	Z	B[a)]
H(4a)	0.8587	-0.0216	0.1895	6.6
H(4b)	0.7243	-0.1388	0.2464	6.6
H(5a)	0.4966	0.0263	0.1410	4.2
H(5b)	0.5766	0.2206	0.1886	4.2
H(9)	0.5235	0.2775	0.9622	2.8
H(10)	0.1508	0.3581	0.9289	3.7

a) Thermal Parameters in the Form of $\exp(-B^*(\sin\theta/\lambda)^2)$

Table 14.

Thermal Parameters of Nonhydrogen Atoms of EVT_2AsF_6 in the Form of $\exp(-(B(11)*h^2+B(22)*k^2+B(33)*l^2+B(12)*h*k+B(13)*h*l+B(23)*k*l))$ and Their Estimated Standard Deviations in Parentheses

Atom	B(11)	B(22)	B(33)	B(12)	B(13)	B(23)
C(1)	0.018(2)	0.0152(8)	0.0028(2)	-0.012(2)	0.0015(7)	-0.0012(6)
C(2)	0.019(2)	0.0157(8)	0.0025(2)	-0.008(2)	0.0028(7)	-0.0009(6)
C(3)	0.021(2)	0.0142(8)	0.0028(2)	-0.011(2)	0.0040(7)	-0.0025(6)
C(4)	0.031(2)	0.044(2)	0.0033(3)	-0.010(3)	0.003(1)	-0.010(2)
C(5)	0.026(2)	0.023(2)	0.0031(2)	-0.011(3)	0.0040(9)	-0.0024(8)
C(6)	0.017(2)	0.0143(8)	0.0026(2)	-0.011(2)	0.0024(7)	-0.0009(6)
C(7)	0.019(2)	0.0126(7)	0.0023(2)	-0.008(2)	0.0023(7)	-0.0013(6)
C(8)	0.018(2)	0.0140(8)	0.0024(2)	-0.008(2)	0.0024(7)	-0.0008(6)
C(9)	0.028(2)	0.0175(9)	0.0026(2)	-0.009(2)	0.0046(8)	0.0011(7)
C(10)	0.029(2)	0.021(2)	0.0030(2)	-0.013(2)	0.0053(9)	0.0015(7)
S(1)	0.0163(3)	0.0222(3)	0.00261(5)	-0.0058(5)	0.0009(2)	-0.0025(2)
S(2)	0.0158(3)	0.0211(3)	0.00269(5)	-0.0117(5)	0.0026(2)	-0.0036(2)
S(3)	0.0181(3)	0.0266(3)	0.00325(5)	-0.0011(5)	0.0038(2)	-0.0039(2)
S(4)	0.0199(3)	0.0303(4)	0.00268(5)	-0.0191(6)	0.0023(2)	-0.0053(2)
S(5)	0.0155(3)	0.0194(3)	0.00258(5)	-0.0044(4)	0.0017(2)	-0.0018(2)
S(6)	0.0153(3)	0.0186(3)	0.00246(4)	-0.0108(4)	0.0013(2)	-0.0012(2)
S(7)	0.0209(4)	0.0224(3)	0.00248(5)	-0.0141(5)	0.0000(2)	-0.0006(2)
S(8)	0.0188(3)	0.0214(3)	0.00316(5)	-0.0012(5)	0.0047(2)	-0.0002(2)
As	0.0179(2)	0.0170(2)	0.00264(3)	-0.0039(3)	0.0024(1)	0.00105(9)
F(1)	0.090(3)	0.0194(8)	0.0079(3)	-0.030(3)	0.016(2)	-0.0056(7)
F(2)	0.0205(9)	0.057(2)	0.0063(2)	-0.003(2)	0.0084(7)	0.0088(8)
F(3)	0.036(2)	0.042(2)	0.0032(2)	0.001(2)	0.0014(6)	0.0049(6)

$w = [\sigma^2(F_o) - 0.0055|F_o| + 0.0029|F_o|^2]^{-1}$ for EVT_2AsF_6. The atomic scattering factors were taken from those of International Tables of X-Ray Crystallography.[69] The final R indices were 0.118 for EVT_2PF_6 and 0.053 for EVT_2AsF_6. The atomic coordinates, equivalent isotropic temperature factors[70] and anisotropic temperature factors are given in Tables 11 and 12 for EVT_2PF_6 and in Tables 13 and 14 for EVT_2AsF_6.

3-2-4 Determination of Molecular and Crystal Structures of $EOTT_2IBr_2$ and $EOTT_2AuI_2$

$EOTT_2IBr_2$: $(C_{10}H_8OS_8)_2IBr_2$, M = 1088.12, triclinic, space group $P\bar{1}$, a = 4.753(1), b = 11.650(4), c = 16.135(5) Å, α = 106.78(2), β = 93,29(1), γ = 83.96(1)°, V= 850.2(4) Å^3, Z = 1, D_c = 2.13 g cm^{-3}, μ(Mo K_α) = 44.0 cm^{-1}; $EOTT_2AuI_2$: $(C_{10}H_8OS_8)_2AuI_2$, M = 1252.18, triclinic, space group $P\bar{1}$, a = 4.792(1), b = 11.568(3), c = 16.332(5) Å, α = 107.53(1), β = 93.62(2), γ = 83.99(2)°, V = 858.2(4) Å^3, Z = 1, D_c = 2.42 g cm^{-3}, μ(Mo K_α) = 72.0 cm^{-1}. The crystals were needle shaped with approximate dimensions of 0.38 x 0.14 x 0.04 mm^3 for $EOTT_2IBr_2$ and 0.42 x 0.19 x 0.04 mm^3 for $EOTT_2AuI_2$. X-ray diffraction data were collected by the θ-2θ scan technique up to 2θ = 55° on a Rigaku AFC-4 four-circle diffractometer, using graphite monochromatized Mo K_α radiation (λ = 0.7107 Å). The scan rates (θ) were 4° min^{-1}, and the scan widths Δθ = (1.7 + 0.5 tanθ)° for $EOTT_2IBr_2$ and Δθ = (1.4 + 0.5 tanθ)° for $EOTT_2AuI_2$. Backgrounds were counted for 4 s at both ends of a

scan. No significant intensity decay of three standard reflections, which were measured after every 100 reflections, were detected for both crystals. For $EOTT_2IBr_2$, of the 4325 reflections measured, 2821 were observed ($|F_o| > 2\sigma(F_o)$). For $EOTT_2AuI_2$, of the 4403 reflections measured, 3346 were observed ($|F_o| > 2\sigma(F_o)$). The data were corrected for Lorentz and polarization factors, but not for absorption.

The structures were solved by the direct method (SHELX-76),[71] and were refined anisotropically by the block-diagonal least-squares procedure (HBLS V).[68] Since the IBr_2^- and AuI_2^- anions were found to be disordered on D-map, it was assumed that 80% of anions are on the center of symmetry and 20% of anions are on the position where the peaks were found on D-map. For $EOTT_2IBr_2$, not all of hydrogen atoms could be reasonably refined, then they were relocated at the calculated positions, and the isotropic temperature factor of each hydrogen atom was assumed equal to the equivalent isotropic temperature factor of the carbon atom to which the hydrogen atom attached. For $EOTT_2AuI_2$, the hydrogen atoms were not included in the final refinement. The function minimized was $\Sigma w(\Delta F)^2$. The weighting functions used in the final stage of the refinements were $w = [\sigma^2(F_o) + 0.0930|F_o| + 0.0015|F_o|^2]^{-1}$ for $EOTT_2IBr_2$ and $w = [\sigma^2(F_o) + 0.1496|F_o| + 0.0019|F_o|^2]^{-1}$ for $EOTT_2AuI_2$. Atomic scattering factors were taken from those of International Tables of X-Ray Crystallography.[69] Final R indices were 0.079 for $EOTT_2IBr_2$ and 0.076 for $EOTT_2AuI_2$. The atomic coordinates, equivalent isotropic temperature factors[70] and anisotropic

Table 15-a.

Atomic Parameters of Nonhydrogen Atoms of $EOTT_2IBr_2$ with Equivalent Isotropic Temperature Factors[70] and Their Estimated Standard Deviations in Parentheses

Atom	x	y	z	$B_{eq}/Å^2$
I	0. (0)	0. (0)	0. (0)	3.0
Br	0.1593(4)	0.2160(2)	-0.0033(1)	4.6
I(1)	-0.003(3)	0.013(2)	0.0291(6)	6.1
Br(1)	0.148(3)	0.223(2)	0.022(1)	5.5
Br(2)	-0.151(3)	-0.203(2)	0.027(1)	5.6
S(1)	-0.0375(6)	0.3212(3)	0.4134(2)	2.8
S(2)	0.2432(6)	0.1240(3)	0.4762(2)	3.0
S(3)	0.2639(7)	0.2544(3)	0.2493(2)	3.9
S(4)	0.6019(7)	0.0202(3)	0.3248(2)	3.8
S(5)	-0.3954(6)	0.4168(3)	0.5913(2)	2.6
S(6)	-0.1171(6)	0.2148(3)	0.6484(2)	2.7
S(7)	-0.7813(6)	0.5018(3)	0.7399(2)	2.8
S(8)	-0.4590(7)	0.2645(3)	0.8052(2)	3.5
C(1)	-0.004(2)	0.2482(8)	0.4940(6)	2.6
C(2)	0.220(2)	0.2232(8)	0.3479(6)	2.5
C(3)	0.346(2)	0.1318(8)	0.3766(6)	2.3
C(4)	0.534(4)	0.147(2)	0.198(1)	6.3
C(5)	0.541(5)	0.030(2)	0.2132(9)	7.3
C(6)	-0.155(2)	0.2887(8)	0.5682(6)	2.1
C(7)	-0.510(2)	0.3983(8)	0.6870(6)	2.3
C(8)	-0.382(2)	0.3066(8)	0.7139(6)	2.3
C(9)	-0.625(3)	0.5638(9)	0.8477(7)	3.3
C(10)	-0.395(3)	0.3994(9)	0.8935(7)	4.0
O	-0.626(2)	0.4906(7)	0.9037(5)	4.0

Table 15-b.

Calculated Positional Parameters and Assumed Thermal Parameters of Hydrogen Atoms of $EOTT_2IBr_2$

Atom	X	Y	Z	B[a)]
H(4a)	0.5101	0.1344	0.1296	6.3
H(4b)	0.7342	0.1823	0.2210	6.3
H(5a)	0.7076	-0.0279	0.1745	7.3
H(5b)	0.3406	-0.0055	0.1902	7.3
H(9a)	-0.7404	0.6494	0.8775	3.3
H(9b)	-0.4078	0.5783	0.8404	3.3
H(10a)	-0.2073	0.4350	0.8804	4.0
H(10b)	-0.3611	0.3746	0.9532	4.0

a) Thermal Parameters in the Form of $\exp(-B^*(\sin\theta/\lambda)^2)$

Table 16.

Thermal Parameters of Nonhydrogen Atoms of $EOTT_2IBr_2$ in the Form of $\exp(-(B(11)*h^2+B(22)*k^2+B(33)*l^2+B(12)*h*k+B(13)*h*l+B(23)*k*l))$ and Their Estimated Standard Deviations in Parentheses

Atom	B(11)	B(22)	B(33)	B(12)	B(13)	B(23)
I	0.0327(5)	0.0081(2)	0.00180(4)	0.0062(4)	0.0050(3)	0.0018(1)
Br	0.063(1)	0.0087(2)	0.00393(7)	0.0005(6)	0.0056(4)	0.0036(2)
I(1)	0.053(5)	0.016(2)	0.0057(6)	0.008(4)	0.004(4)	0.006(2)
Br(1)	0.050(7)	0.014(2)	0.0056(7)	-0.008(6)	-0.002(4)	0.005(2)
Br(2)	0.048(7)	0.014(2)	0.0060(7)	0.000(6)	-0.001(4)	0.006(2)
S(1)	0.035(2)	0.0051(2)	0.0029(1)	0.0059(8)	0.0048(6)	0.0030(3)
S(2)	0.036(2)	0.0056(2)	0.0031(1)	0.0077(8)	0.0026(6)	0.0029(3)
S(3)	0.051(2)	0.0077(3)	0.0039(2)	0.004(1)	0.0113(7)	0.0049(3)
S(4)	0.039(2)	0.0060(3)	0.0047(2)	0.0102(9)	0.0077(7)	0.0017(3)
S(5)	0.031(2)	0.0048(2)	0.0027(1)	0.0045(8)	0.0025(6)	0.0033(3)
S(6)	0.037(2)	0.0048(2)	0.00253(9)	0.0076(8)	0.0020(6)	0.0023(3)
S(7)	0.027(2)	0.0053(2)	0.0033(2)	0.0034(8)	0.0035(6)	0.0021(3)
S(8)	0.066(2)	0.0046(2)	0.0028(1)	-0.003(1)	0.0052(7)	0.0025(3)
C(1)	0.029(5)	0.0044(8)	0.0032(4)	-0.000(3)	0.001(3)	0.0024(9)
C(2)	0.028(5)	0.0044(8)	0.0025(4)	-0.004(3)	0.004(2)	-0.0007(9)
C(3)	0.019(4)	0.0034(7)	0.0032(4)	-0.001(3)	0.000(2)	0.0006(9)
C(4)	0.08(1)	0.012(2)	0.0067(8)	0.031(7)	0.019(5)	0.009(2)
C(5)	0.16(2)	0.005(1)	0.0052(7)	0.001(7)	0.038(6)	0.001(2)
C(6)	0.023(4)	0.0042(7)	0.0023(4)	-0.003(3)	-0.002(2)	0.0017(8)
C(7)	0.025(4)	0.0053(8)	0.0023(4)	-0.002(3)	-0.000(2)	0.0027(9)
C(8)	0.029(5)	0.0045(7)	0.0023(4)	-0.001(3)	0.004(2)	0.0021(8)
C(9)	0.048(6)	0.0053(9)	0.0031(5)	-0.002(4)	0.002(3)	0.002(1)
C(10)	0.059(7)	0.0047(9)	0.0038(5)	0.008(4)	0.001(3)	0.000(1)
O	0.061(5)	0.0067(7)	0.0034(4)	-0.003(3)	0.007(2)	0.0021(8)

Table 17.

Atomic Parameters of Nonhydrogen Atoms of $EOTT_2AuI_2$ with Equivalent Isotropic Temperature Factors[70] and Their Estimated Standard Deviations in Parentheses

Atom	x	y	z	$B_{eq}/Å^2$
Au	0. (0)	0. (0)	0. (0)	3.9
I	-0.1589(3)	-0.2000(1)	0.0083(1)	4.6
Au(1)	0.041(3)	0.013(2)	0.0247(8)	10.5
I(1)	0.179(2)	0.215(2)	0.006(2)	8.2
I(2)	-0.103(2)	-0.1836(9)	0.0225(8)	6.2
S(1)	-0.0396(6)	0.3185(3)	0.4139(2)	3.1
S(2)	0.2424(6)	0.1252(3)	0.4800(2)	3.1
S(3)	0.2579(7)	0.2402(3)	0.2501(2)	4.2
S(4)	0.5959(7)	0.0130(3)	0.3319(2)	4.1
S(5)	-0.3971(5)	0.4201(3)	0.5901(2)	2.8
S(6)	-0.1155(6)	0.2198(3)	0.6487(2)	3.0
S(7)	-0.7791(5)	0.5081(3)	0.7380(2)	3.0
S(8)	-0.4534(7)	0.2723(3)	0.8038(2)	3.7
C(1)	-0.003(2)	0.2504(8)	0.4959(6)	2.6
C(2)	0.213(2)	0.2182(8)	0.3489(6)	2.7
C(3)	0.342(2)	0.1268(9)	0.3793(7)	3.0
C(4)	0.485(5)	0.115(3)	0.199(2)	13
C(5)	0.596(7)	0.026(2)	0.225(2)	12
C(6)	-0.157(2)	0.2907(8)	0.5678(6)	2.5
C(7)	-0.510(2)	0.4045(8)	0.6877(6)	2.5
C(8)	-0.377(2)	0.3120(8)	0.7129(6)	2.7
C(9)	-0.615(3)	0.5750(9)	0.8441(7)	4.1
C(10)	-0.394(3)	0.410(1)	0.8892(7)	4.0
O	-0.613(2)	0.5042(7)	0.9003(5)	4.1

Table 18.

Thermal Parameters of Nonhydrogen Atoms of $EOTT_2AuI_2$ in the Form of $\exp(-(B(11)*h^2+B(22)*k^2+B(33)*l^2+B(12)*h*k+B(13)*h*l+B(23)*k*l))$ and Their Estimated Standard Deviations in Parentheses

Atom	B(11)	B(22)	B(33)	B(12)	B(13)	B(23)
Au	0.0436(4)	0.00900(7)	0.00324(3)	-0.0008(3)	-0.0002(2)	0.00215(7)
I	0.0594(6)	0.00940(9)	0.00359(4)	-0.0042(4)	0.0040(3)	0.0021(1)
Au(1)	0.093(6)	0.021(2)	0.0142(9)	-0.034(5)	-0.044(4)	0.015(2)
I(1)	0.028(4)	0.017(2)	0.014(1)	-0.016(4)	-0.013(3)	0.008(2)
I(2)	0.047(4)	0.0095(8)	0.0087(6)	0.007(3)	-0.014(3)	0.002(2)
S(1)	0.038(2)	0.0059(2)	0.0032(1)	0.0096(8)	0.0057(5)	0.0040(3)
S(2)	0.040(2)	0.0056(2)	0.00303(9)	0.0097(8)	0.0041(5)	0.0032(3)
S(3)	0.054(2)	0.0090(3)	0.0040(2)	0.005(1)	0.0115(7)	0.0061(3)
S(4)	0.044(2)	0.0067(3)	0.0049(2)	0.0118(9)	0.0092(7)	0.0023(3)
S(5)	0.036(2)	0.0051(2)	0.00292(9)	0.0060(7)	0.0034(5)	0.0037(2)
S(6)	0.041(2)	0.0051(2)	0.00285(9)	0.0093(7)	0.0035(5)	0.0033(2)
S(7)	0.031(1)	0.0054(2)	0.0035(1)	0.0053(7)	0.0052(5)	0.0023(3)
S(8)	0.066(2)	0.0053(2)	0.0029(1)	-0.0021(9)	0.0058(7)	0.0034(3)
C(1)	0.031(4)	0.0047(7)	0.0027(4)	-0.000(3)	0.002(2)	0.0027(8)
C(2)	0.030(4)	0.0047(7)	0.0034(4)	-0.001(3)	0.004(2)	0.0023(9)
C(3)	0.028(4)	0.0050(7)	0.0038(5)	0.006(3)	0.005(2)	0.0022(9)
C(4)	0.13(2)	0.041(5)	0.0053(8)	0.12(2)	0.033(6)	0.018(4)
C(5)	0.26(3)	0.009(2)	0.010(2)	0.05(2)	0.08(2)	0.012(3)
C(6)	0.031(4)	0.0052(7)	0.0023(4)	0.001(3)	0.000(2)	0.0019(8)
C(7)	0.026(4)	0.0048(7)	0.0029(4)	-0.002(3)	0.004(2)	0.0019(8)
C(8)	0.036(5)	0.0052(7)	0.0022(4)	0.000(3)	0.001(2)	0.0024(8)
C(9)	0.069(7)	0.0050(8)	0.0033(5)	0.005(4)	0.007(3)	0.001(1)
C(10)	0.061(7)	0.0073(9)	0.0027(4)	-0.001(4)	-0.000(3)	0.002(1)
O	0.064(5)	0.0067(7)	0.0032(3)	0.002(3)	0.010(2)	0.0026(7)

temperature factors are given in Tables 15 and 16 for $EOTT_2IBr_2$ and in Tables 17 and 18 for $EOTT_2AuI_2$.

3-3 Molecular and Crystal structures of neutral TMTVT

The TMTVT molecule has an inversion center at the midpoint between the two central carbon atoms, and is on the center of symmetry in the crystal. The central C_6S_8 portion of the TMTVT molecule is approximately planar and the two bis(methylthio)-vinylene portions at both ends of the molecule are bent toward opposite directions from each other (Fig. 2). Both BEDT-TTF[72] and bis(vinylenedithio)tetrathiafulvalene (VT)[61] possess planar structures only at the central C_2S_4 portion. Comparing the molecular structure of TMTVT with those of BEDT-TTF and VT, the central planar portion is extended more widely in the former molecule. The crystal structure is characterized by a face-to-face stack of TMTVT molecules along the c-axis with equal intermolecular spacings (Fig. 3(a)). The interplanar distance between adjacent molecules is 3.41 Å. The S-S contacts [3.700(3) Å] which are almost equal to the van der Waals radius (3.7 Å) are formed between the methylthio groups in TMTVT molecules belonging to the adjacent stacks [S(5)(x,y,z)••• S(6)(-0.5+x,0.5-y,-0.5+z)]: these are shown by dotted lines in Fig. 3. All of the other S-S distances are longer than the van der Waals radius. Fig. 3(b) shows a side-by-side arrangement of molecules of equal height. All of the side-by-side S-S

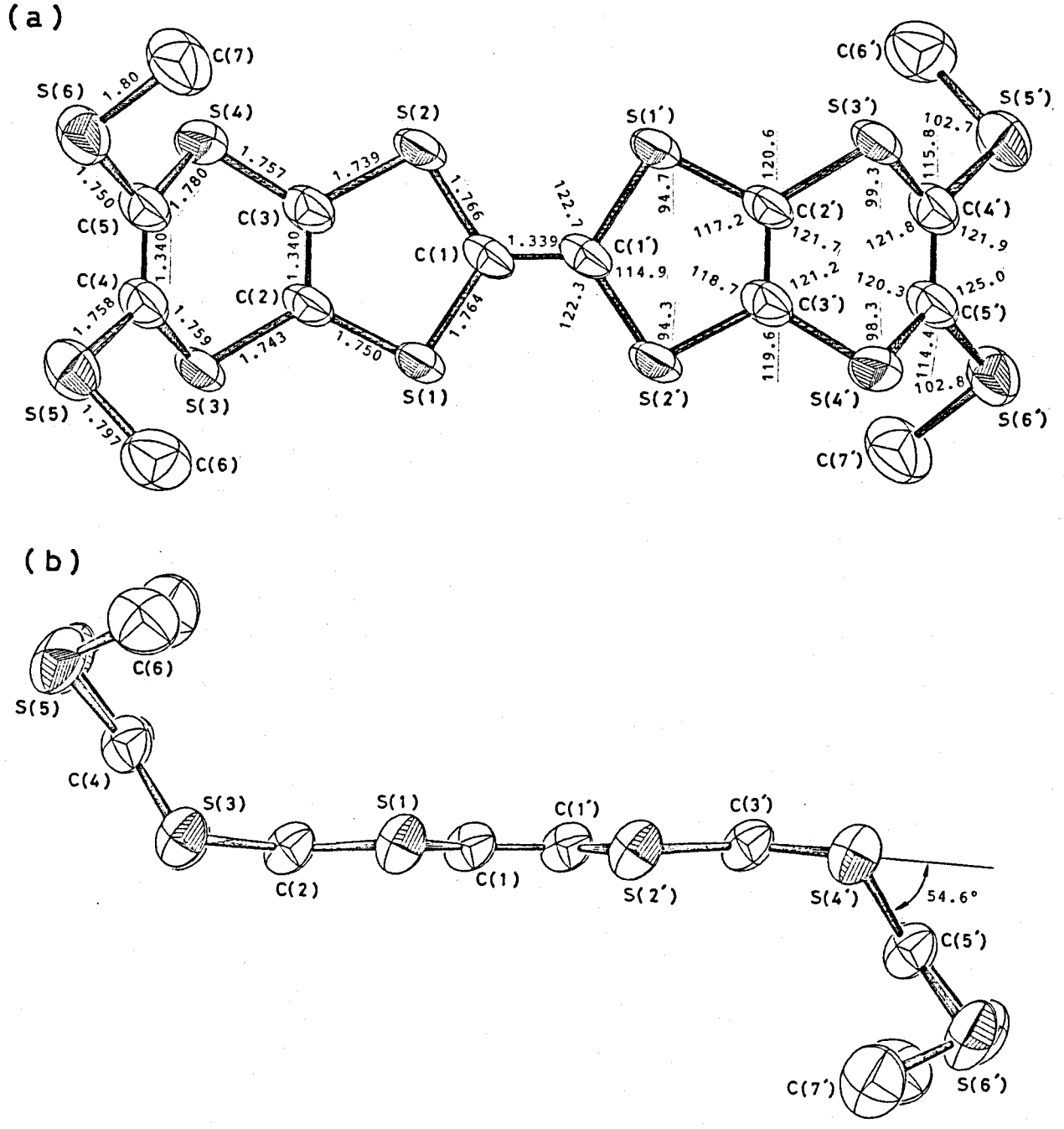

Fig. 2. Molecular structure of TMTVT.[75] (a) Over view, (b) side view. Nonhydrogen atoms are drawn as thermal ellipsoids with 50% probability level. Estimated standard deviations of the bond lengths and bond angles are 0.005-0.01 Å and 0.3-0.4°, respectively.

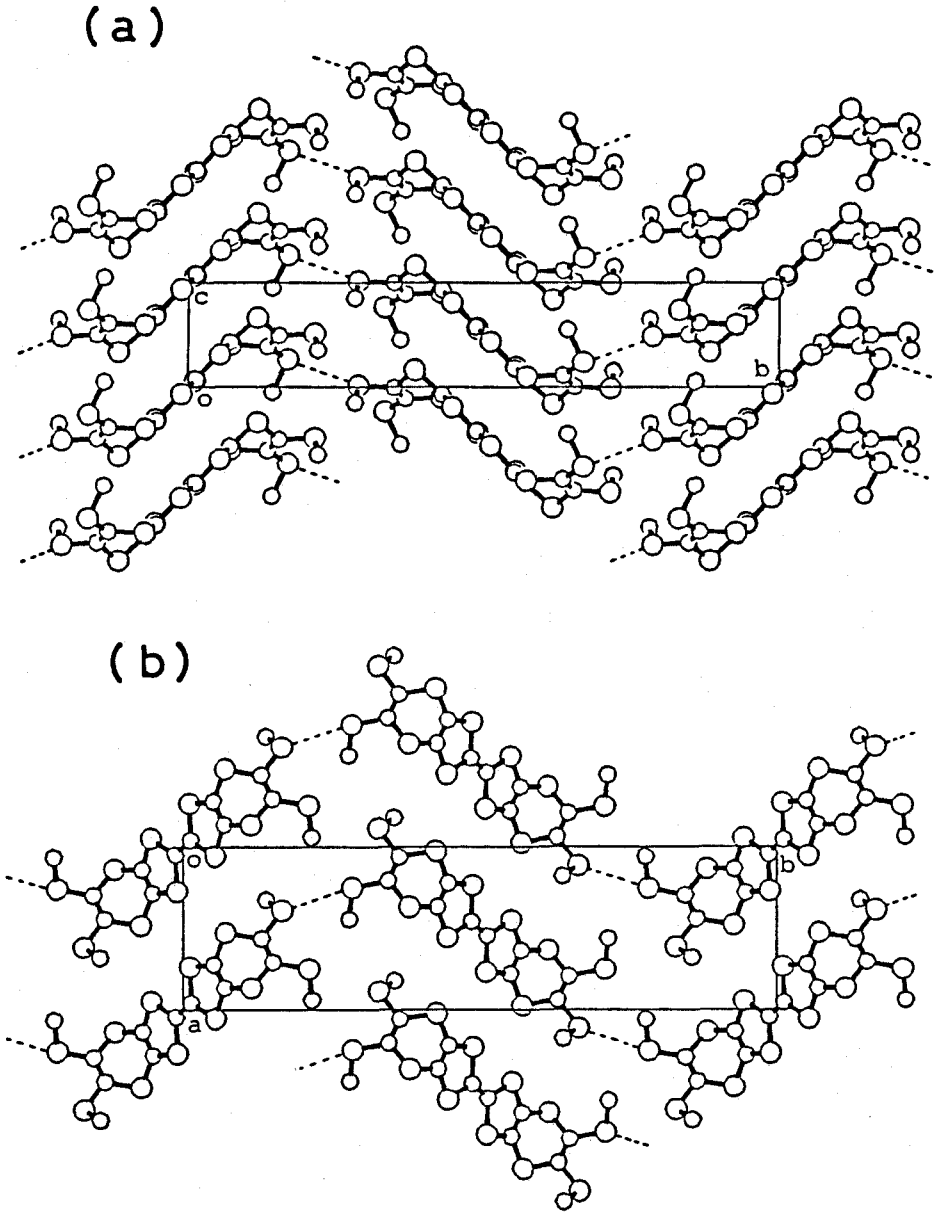

Fig. 3. Crystal structure of TMTVT[76] projected along the a axis (a) and the c axis (b). Dotted line indicates intermolecular S-S contact almost equal to the van der Waals distance (3.7 Å).

distances are longer than the van der Waals radius, unlike the cases of BEDT-TTF salts.[30] Fig. 4 shows the overlap of two TMTVT molecules projected normal to the molecular plane. The adjacent molecules in a stack are shifted in order to avoid direct overlap of carbon and sulfur atoms between them.

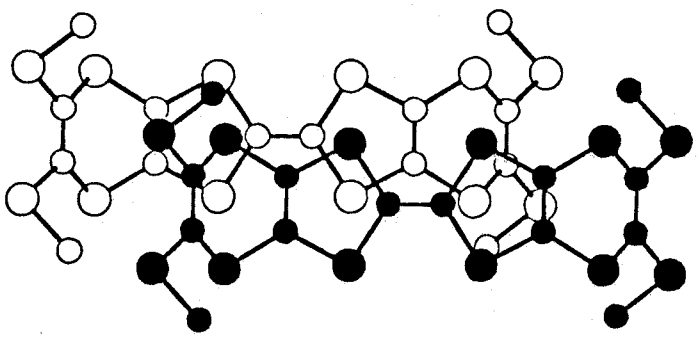

Fig. 4. Overlap of two TMTVT molecules.[76]

3-4 Molecular and Crystal structures of neutral EVT

The EVT molecule is not planar (Fig. 5). The central C_2S_4 portion is almost planar, but both of the outer parts are bent in the same direction. This molecular structure is much closer to that of BEDT-TTF[72] than to that of VT; the outer parts of VT are bent in the opposite directions.[61] The pair-by-pair arrangement of EVT molecules, related by a center of symmetry, is shown in Fig. 6. The molecular arrangement is very close to that in the BEDT-TTF crystal.[72] The mode of overlapping of the paired molecules is shown in Fig. 7(a). The mode of the overlapping of the two molecules is also very close to that of

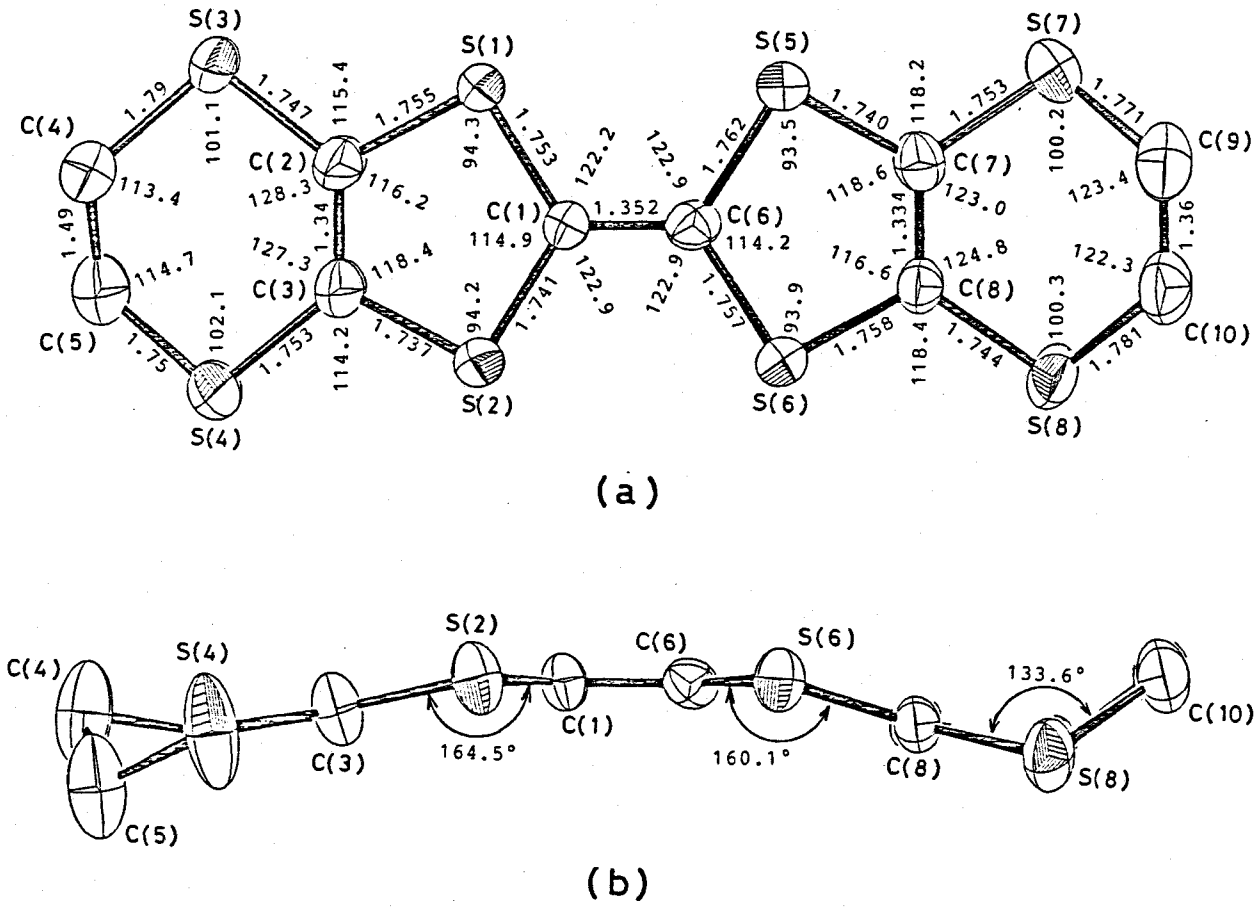

Fig. 5. Molecular structure of EVT.[75] (a) Over view, (b) side view. Nonhydrogen atoms are drawn as thermal ellipsoids with 50% probability level. Estimated standard deviations of the bond lengths and bond angles are 0.006-0.02 Å and 0.3-0.7°, respectively.

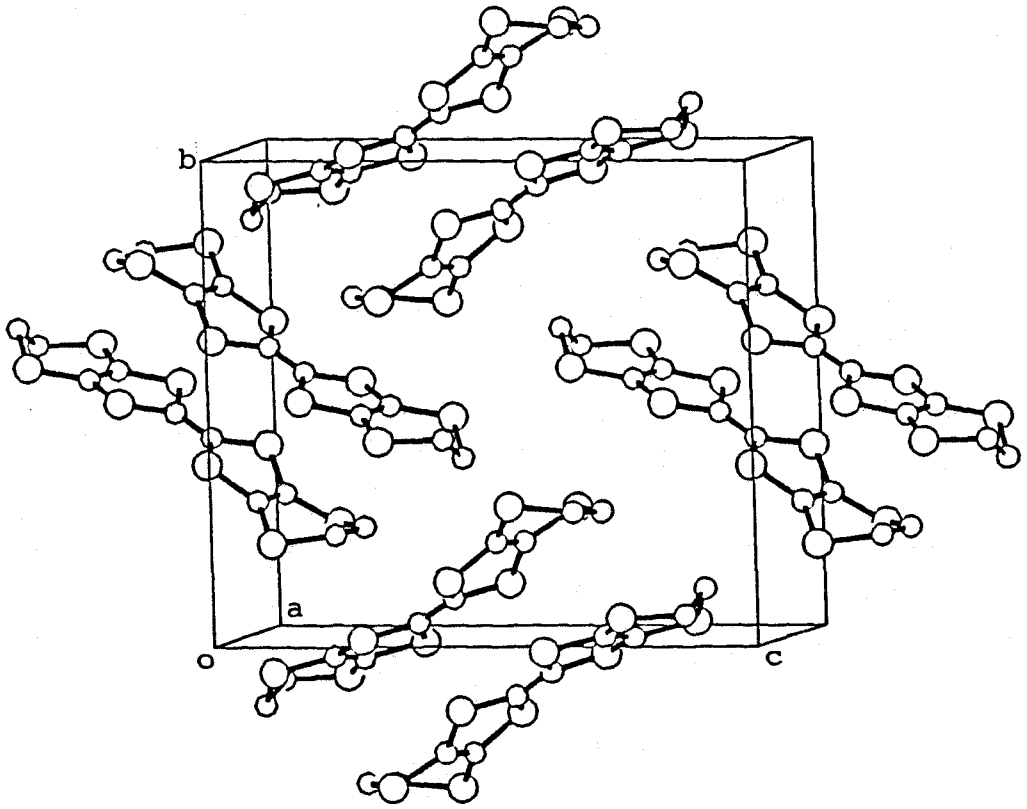

Fig. 6. Crystal structure of EVT.[76]

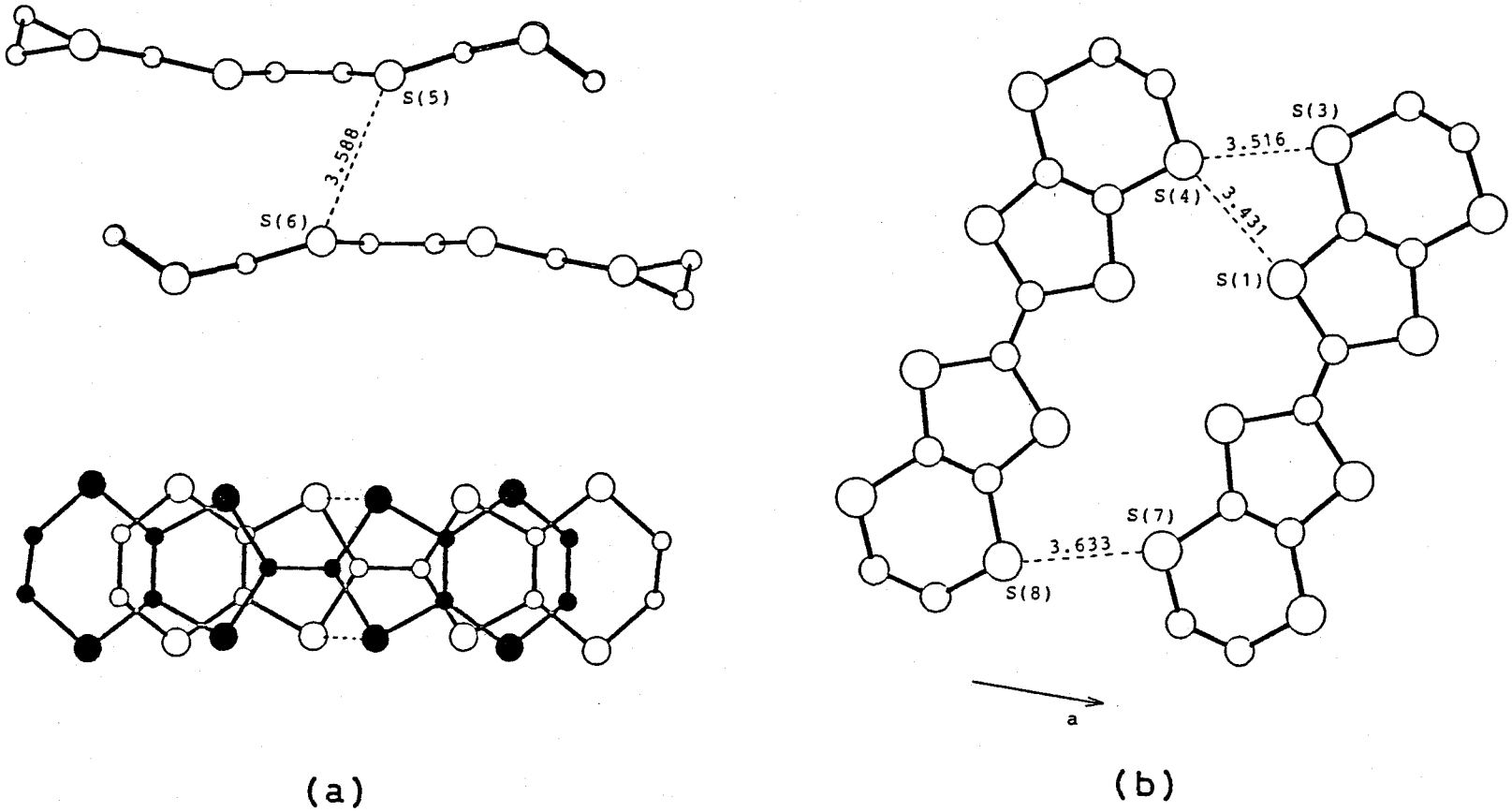

Fig. 7. (a) The mode of overlapping of the paired EVT molecules.[76] The dotted line indicates the S-S contacts shorter than the van der Waals distance (3.7 Å). (b) Molecular arrangement along the a axis.[76]

BEDT-TTF.[72] Several intermolecular S-S distances [S(5)(x,y,z)•••S(6)(-x,-y,1-z)(= 3.588(3) Å), S(1)(x,y,z)••• S(4)(-1+x, y,z)(= 3.431(4) Å), S(3)(x,y,z)•••S(4)(-1+x,y,z)(= 3.516(4) Å), and S(7)(x,y,z)•••S(8)(-1+x,y,z)(= 3.633(3) Å)] are shorter than the van der Waals distance (3.7 Å) (Figs. 7).

3-5 Molecular and Crystal structures of EVT_2PF_6 and EVT_2AsF_6

Fig. 8 shows the molecular structure of the EVT molecule in the EVT_2AsF_6 crystal, together with the bond lengths and bond angles. The planarity of the EVT molecule was increased in its semication state ($EVT^{+0.5}$). No conformational disorder was found at the ethylene group of the EVT molecule. Fig. 9 shows the crystal structure of EVT_2AsF_6. Only one EVT molecule is crystallographically independent, and the AsF_6^- anion is on the center of symmetry. The EVT molecules are stacked along the b axis, as is usually observed for the conducting salts of TTF derivatives (Fig. 9). Two kinds of the molecular overlap shown in Figs. 10(a) and 10(b) are observed. In one overlap mode (Fig. 10(a)), two EVT molecules are slightly shifted relative to each other within the unit cell. In the other overlap mode (Fig. 10(b)), the five-membered ring of one EVT molecule is overlapped with the six-membered ring of another EVT molecule across the unit cell. These two overlap modes are characterized by l_1 and l_2 in Figs. 10(a) and 10(b). No intermolecular S-S contact shorter than the van der Waals

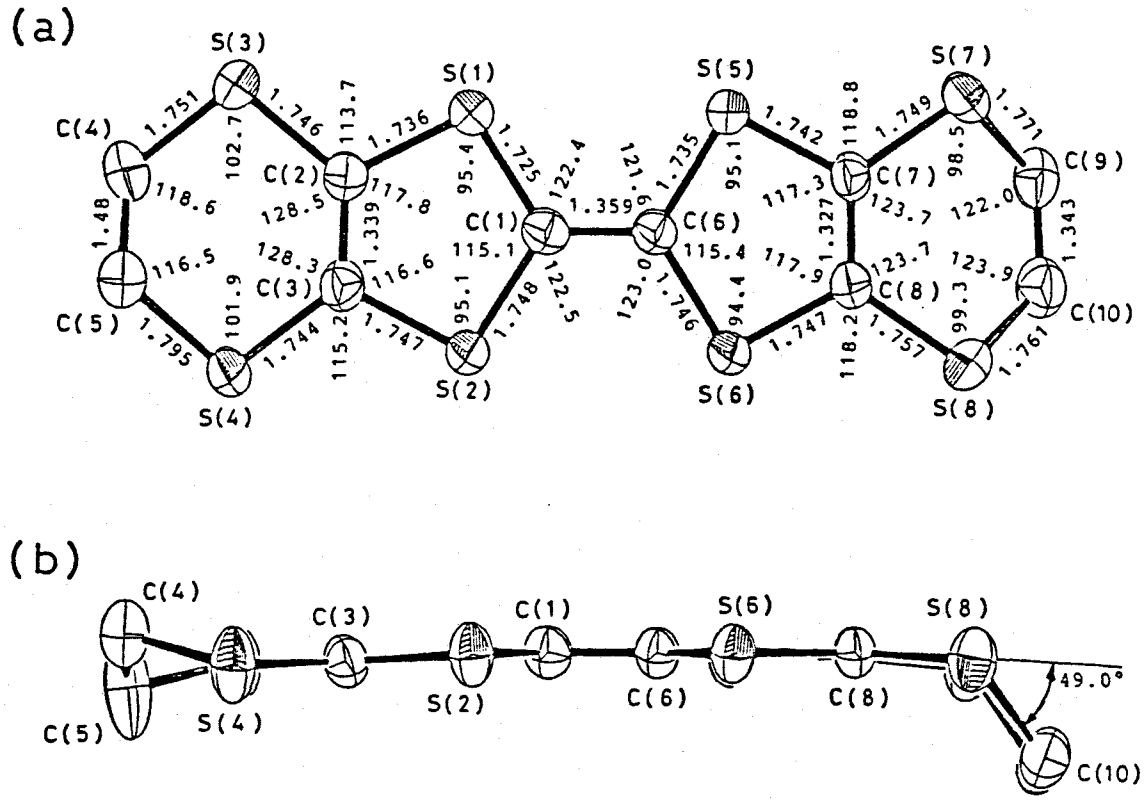

Fig. 8. Molecular structure of EVT molecule in EVT_2AsF_6.[75]
(a) Over view, (b) side view. Nonhydrogen atoms are drawn as thermal ellipsoids with 50% probability level. Estimated standard deviations of the bond lengths and bond angles are 0.005-0.02 Å and 0.3-0.6°, respectively.

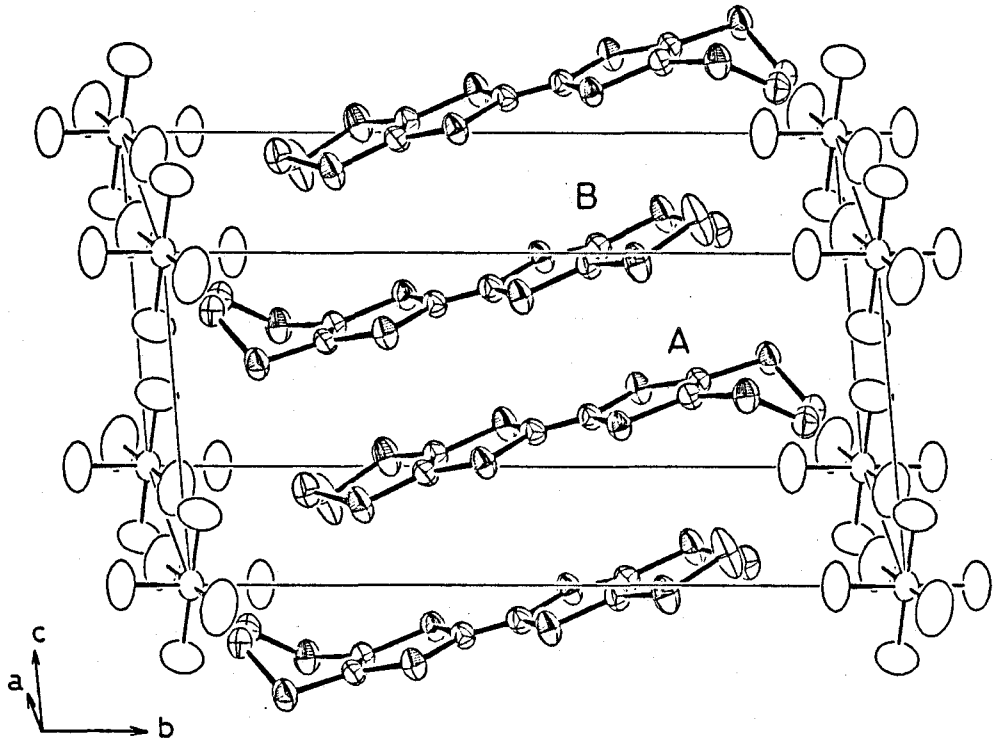

Fig. 9. Crystal structure of EVT_2AsF_6.[75] The molecules A and B are related by the symmetry operation (1-x, 1-y, 1-z).

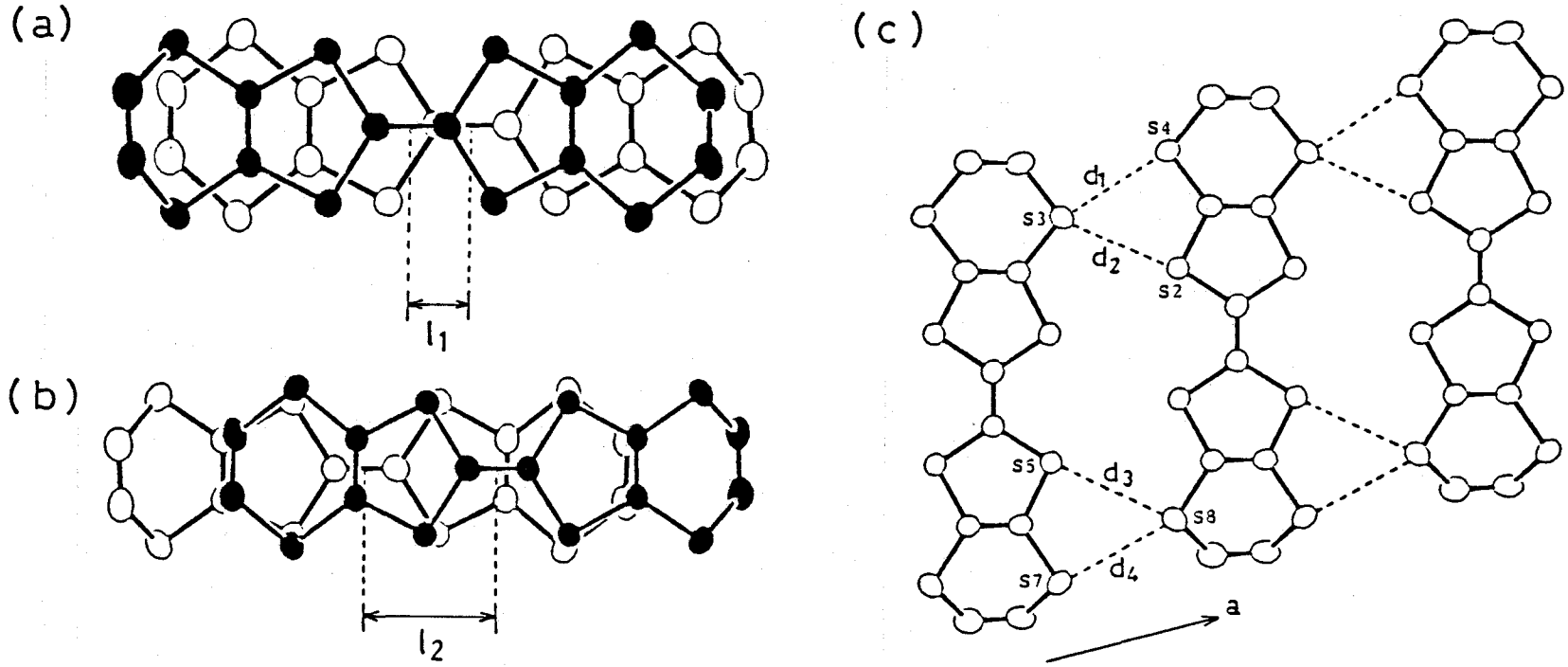

Fig. 10. (a) The mode of a stacking of EVT molecules in EVT_2AsF_6 related by the symmetry operation (1-x, 1-y, 1-z). (b) The mode of a stacking of EVT molecules related by the symmetry operation (1-x, -y, 1-z).
(c) The arrangement of EVT molecules along the a axis. The dotted line indicates the S-S contacts shorter than the van der Waals distance (3.7 Å). The values of l_1, l_2, d_1, d_2, d_3, and d_4 are summarized in Table 19.

Table 19.
Relative Shift of Donor Molecules (l_1 and l_2) and Intercolumnar S-S Distances between Donor Molecules (d_1, d_2, d_3, and d_4) in the Crystals of α-$(BEDT\text{-}TTF)_2PF_6$, EVT_2PF_6, EVT_2AsF_6, and VT_2PF_6.

Distance[a)]	α-$(BEDT\text{-}TTF)_2PF_6$	EVT_2PF_6	EVT_2AsF_6	VT_2PF_6
l_1/Å	0.3	1.2	1.2	1.6
l_2	4.2	3.0	3.0	2.4
d_1	3.48	3.404(7)	3.394(3)	3.51
d_2	3.61	3.450(6)	3.503(2)	3.56
d_3	3.57	3.619(5)	3.664(2)	3.71
d_4	3.58	3.599(6)	3.592(2)	3.43

a) The distances l_1, l_2, d_1, d_2, d_3, and d_4 are shown in Figs. 10(a), 10(b), and 10(c) for EVT_2AsF_6 as typical examples.

distance (3.7 Å) was found within the donor column. This fact is in contrast with the crystal structures of α-$(BEDT\text{-}TTF)_2PF_6$ and VT_2PF_6; intermolecular S-S contacts shorter than 3.7 Å were found within the donor column for these salts.[61,73] Table 19 shows the relative shifts of the donor molecules (l_1 and l_2) and intercolumnar S-S distances (d_1, d_2, d_3, and d_4) in α-$(BEDT\text{-}TTF)_2PF_6$, EVT_2PF_6, EVT_2AsF_6, and VT_2PF_6 for the sake of a comparison (see also Figs. 10(a), 10(b), and 10(c)). All of the S-S contacts along the a-axis were shorter than 3.7 Å in EVT_2AsF_6, as shown in Fig. 10(c) and Table 19. Both α-$(BEDT\text{-}TTF)_2PF_6$ and VT_2PF_6 also possess intercolumnar S-S contacts shorter than 3.7 Å.[61,73] The molecular and crystal structures of EVT_2PF_6 were found to be very similar to those of EVT_2AsF_6. Hence, the above arguments regarding the molecular and crystal structures of EVT_2AsF_6 are also applicable to the case of EVT_2PF_6. However, the final R value of the latter-mentioned salt was large (R = 0.118) due to poor crystal quality.

3-6 Band Electronic Structures of EVT_2PF_6 and EVT_2AsF_6

Fig. 11 shows intermolecular overlap integrals, Fermi surface, and the band structure of EVT_2PF_6 calculated by a tight-binding approximation based on an extended Hückel molecular orbital. The band structure and Fermi surfaces of EVT_2AsF_6 were very similar to those of EVT_2PF_6. We also

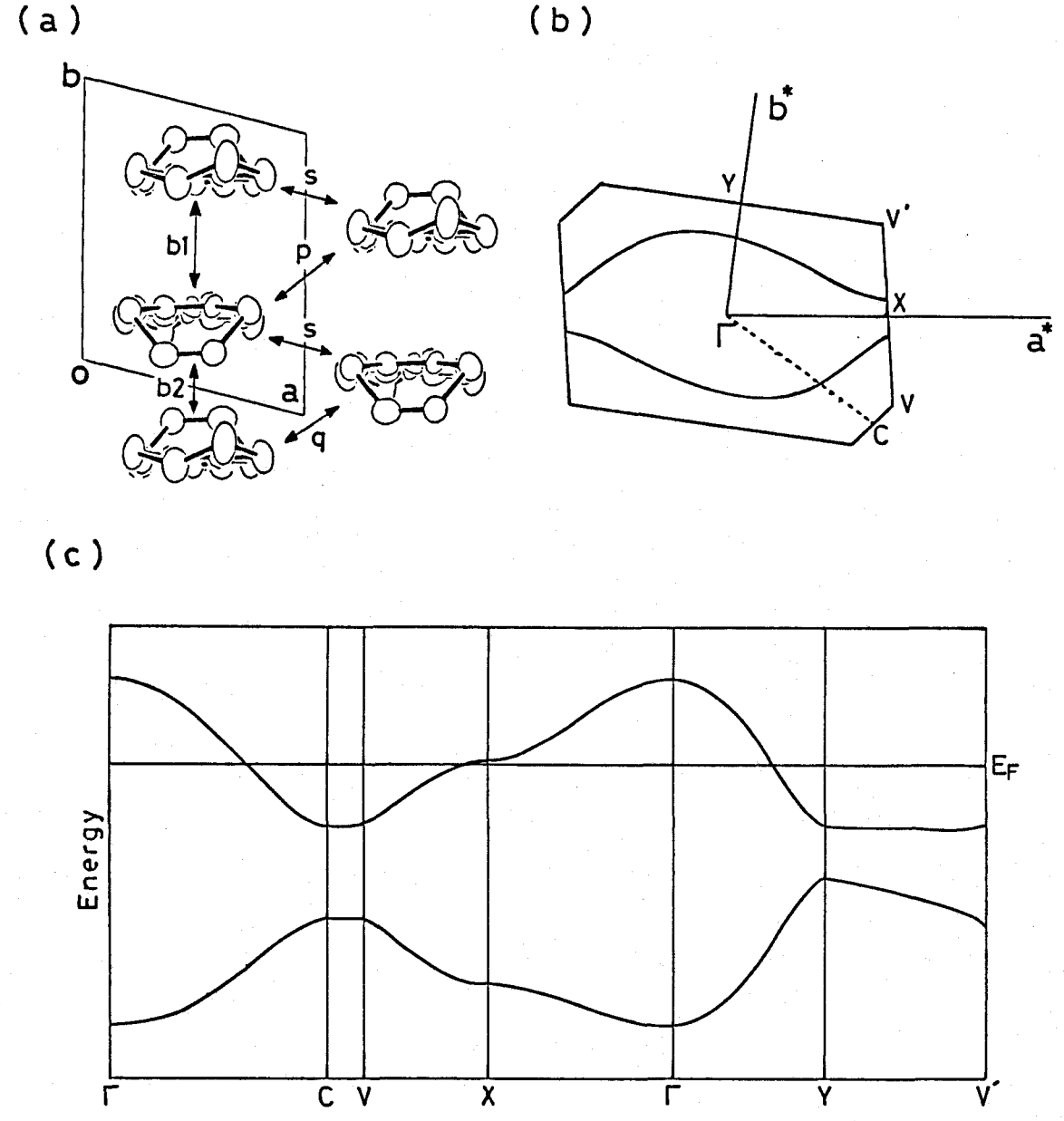

Fig. 11. (a) Intermolecular overlap integrals (b1, b2, p, q, and s), (b) Fermi surface, and (c) band structure of EVT_2PF_6. Since this salt shows a semiconducting behavior, the absence of the band gap (in other words, the appearance of the Fermi surface) will be caused by the neglect of on-site Coulomb repulsion among conducting electrons in the present calculation.

obtained both closed and open Fermi surfaces for α-(BEDT-TTF)$_2$PF$_6$ and VT$_2$PF$_6$,[61], respectively. The appearance of the Fermi surfaces in α-(BEDT-TTF)$_2$PF$_6$, EVT$_2$PF$_6$, and EVT$_2$AsF$_6$ conflicts with their semiconducting properties. These contradictory results are caused by an on-site Coulomb repulsion among conducting electrons, which was not taken into account in the present calculation. Since the present calculation method gives a simple perspective concerning the dimensionality of many conducting organic salts,[74] the following analysis is believed to be valid for any discussion about the relative band electronic structures of BEDT-TTF-, EVT-, and VT-salts. The values of intermolecular overlap integrals of HOMO levels in VT$_2$PF$_6$, EVT$_2$PF$_6$, EVT$_2$AsF$_6$, and α-(BEDT-TTF)$_2$PF$_6$ are summarized in Table 20. Here, the intermolecular overlap integrals (b1, b2, p, q, and s) in EVT$_2$PF$_6$ are shown in Fig. 11 as a typical example. The amount of the intermolecular transfer integral (t) is assumed to be of the order of t = ES [E = orbital energy of HOMO level (≃ -8.5 eV); S = intermolecular overlap integral]. Table 20 shows that a dimeric intermolecular interaction exists in the direction of the donor stack in α-(BEDT-TTF)$_2$PF$_6$; b1 is more than twice as large as b2. The ratio of b1/b2 decreases systematically in the order α-(BEDT-TTF)$_2$PF$_6$ > EVT$_2$PF$_6$ > VT$_2$PF$_6$. Thus, an almost homogeneous intermolecular interaction within the donor column was found for VT$_2$PF$_6$ (b1 b2). This feature makes the effective band width of VT$_2$PF$_6$ the largest among these salts; this is related to the fact that only VT$_2$PF$_6$ shows a metal-like behavior. α-(BEDT-TTF)$_2$PF$_6$ has a much larger

Table 20.

Intermolecular Overlap Integrals of HOMO Calculated by an Extended Hückel Molecular Orbital Method[a)]

Overlap integral	α-(BEDT-TTF)$_2$PF$_6$	EVT$_2$PF$_6$	EVT$_2$AsF$_6$	VT$_2$PF$_6$
b1 x 10^3	20.2	14.5	14.5	13.2
b2 x 10^3	8.7	8.4	8.6	13.9
p x 10^3	2.9	1.8	1.6	2.1
q x 10^3	0.6	3.0	3.3	1.3
s x 10^3	-2.5	-1.0	-0.8	-1.4

a) Overlap integrals b1, b2, p, q, and s are shown in Fig. 11 for EVT$_2$PF$_6$ as a typical example.

absolute value of the overlap integral s than those of the other salts; s is a measure of the side-by-side intermolecular interaction. The dimensionality of the band electronic structure of these salts is discussed below from the viewpoint of their conduction band widths.

The matrix elements (H_{ij}) of a secular equation of α-(BEDT- TTF)$_2$PF$_6$, EVT$_2$PF$_6$, EVT$_2$AsF$_6$, and VT$_2$PF$_6$ are written as follows (see also Fig. 11):

$$H_{11} = H_{22} = 2t_s \cos(ka)$$

and

$$H_{12} = H_{21}^{*} = t_{b1} + t_{b2}e^{-ikb} + t_p e^{ika} + t_q e^{-i(ka+kb)}.$$

Here, t_x (x = b1, b2, p, q, and s) denotes the intermolecular transfer integral. By solving the secular equation, we obtained the following equations for the conduction-band widths (ΔW), important measures for the dimensionality of the band electronic structures of the conducting salts:

$$\Delta W_{\Gamma-Y} = -2(t_{b2} + t_q)$$

and

$$\Delta W_{\Gamma-X} = 4t_s - 2(t_p + t_q).$$

$\Delta W_{\Gamma-Y}$ and $\Delta W_{\Gamma-X}$ are the conduction-band widths in the Γ-Y and Γ-X directions in the Brillouin zone (see Fig. 11). Since the transfer integrals t_x (x = b1, b2, p, q, and s) are of the order of ES (E = orbital energy of HOMO level) and the values of E are not very different from one another for BEDT-TTF, EVT, and VT, the overlap integrals are adopted for the calculations of the band widths. Table 21 summarizes the relative values of the conduction band widths ($\Delta W_{\Gamma-Y}$ and $\Delta W_{\Gamma-X}$) of α-(BEDT-TTF)$_2$PF$_6$,

Table 21.
Relative Conduction Band Widths of α-$(BEDT\text{-}TTF)_2PF_6$, EVT_2PF_6, EVT_2AsF_6, and VT_2PF_6

Salt	$\Delta W_{\Gamma-Y}$	$\Delta W_{\Gamma-X}$
α-$(BEDT\text{-}TTF)_2PF_6$	18.6	17.0
EVT_2PF_6	22.8	13.6
EVT_2AsF_6	23.8	13.0
VT_2PF_6	30.4	12.4

EVT_2PF_6, EVT_2AsF_6, and VT_2PF_6. It is noticeable that $W_{\Gamma-Y}$ increases in the order α-$(BEDT\text{-}TTF)_2PF_6$ < EVT_2PF_6 < VT_2PF_6. On the other hand, $\Delta W_{\Gamma-X}$ changes in the reverse order. Since $\Delta W_{\Gamma-Y}$ and $\Delta W_{\Gamma-X}$ are comparable in α-$(BEDT\text{-}TTF)_2PF_6$, this salt is assumed to possess a two-dimensional electronic property. Table 21 shows that the extent of the two-dimensional nature is largest for α-$(BEDT\text{-}TTF)_2PF_6$, intermediate for EVT_2PF_6, and smallest for VT_2PF_6. The relation between the conduction band widths and the crystal structures are discussed below in more detail regarding these salts.

The $\Delta W_{\Gamma-X}$ value of α-$(BEDT\text{-}TTF)_2PF_6$ is the largest among those of the conducting salts given in Table 21. The main reason for this arises from the largest absolute overlap integral s of this salt (Table 20). All of the HOMO levels of BEDT-TTF, EVT, and VT have larger LCAO coefficients on the sulfur atoms than those on the carbon atoms. Thus, the overlap integral, s, is mainly determined by the side-by-side overlap between the lone-pair orbitals of the sulfur atoms belonging to the adjacent donor columns. The main reason that the $\Delta W_{\Gamma-Y}$ value for EVT_2PF_6 is larger than that for α-$(BEDT\text{-}TTF)_2PF_6$ arises from the larger value of q in the former salt. Here, q denotes the intercolumnar molecular overlap integral between the donor molecules related by a symmetry operation (1-x, -y, -z). On the other hand, EVT salts have smaller values of $\Delta W_{\Gamma-X}$ than those of α-$(BEDT\text{-}TTF)_2PF_6$. Thus, the extent of the two-dimensional nature of the former salts is less than that of the latter. In the case of VT_2PF_6, $\Delta W_{\Gamma-Y}$ is much larger than

those of the corresponding BEDT-TTF and EVT salts. The main reason for this arises from the largest value of b2 (intracolumnar molecular overlap integral). The mode of the stacking of the donor molecules connected by the overlap integral b2 are characterized by l_2 in Table 19. In the case of α-$(BEDT\text{-}TTF)_2PF_6$, the mode of the intermolecular overlap is that of a "ring-external bond-type overlap" usually found in 1-D organic metals. On the other hand, a six-membered ring of one molecule overlaps with a five-membered ring of another molecule in EVT_2PF_6 and VT_2PF_6; the extent of the molecular overlap of the latter salts is larger than that of the former. These features are characterized by the order of l_2 values: α-$(BEDT\text{-}TTF)_2PF_6$ > EVT_2PF_6 > VT_2PF_6. Moreover, only VT_2PF_6 has four S-S contacts shorter than the van der Waals distance between the donor molecules connected by the overlap integral, b2. Since the terminal vinylene group of a VT molecule is less sterically crowded than the terminal ethylene group of a BEDT-TTF or an EVT molecule, especially in the presence of PF_6^- anion nearby, the VT molecules related by a symmetry operation (1-x, -y, -z) are stacked more closely than the latter molecules in EVT_2PF_6 or α-$(BEDT\text{-}TTF)_2PF_6$; this gives rise to the largest value of b2 for the former salt. On the other hand, the intercolumnar overlap integrals (p, q, and s) of VT_2PF_6 are not very different from the corresponding values of the EVT salt; the $\Delta W_{\Gamma\text{-}X}$ value of VT_2PF_6 is similar to that of the EVT salt. Therefore, the extent of the one-dimensional band electronic property of VT_2PF_6 is the largest among the conducting salts

listed in Table 21.

The temperature dependence of electrical conductivities of VT_2PF_6 has been measured. The salt shows a metal-insulator transition at 180 K.[77] The temperature dependence of the X-ray crystallographic analysis of VT_2PF_6 revealed a doubling of the lattice constants below 170 K [(a,b,c)→(2a,2b,2c)].[77] These results are assumed to be caused by the quasi-one-dimensional nature of the VT-salts. Since the extent of the two-dimensional nature of the EVT-salts is expected to be greater than that of the VT-salts, as in the present study, and since EVT is the molecule with the slightest modification of BEDT-TTF, EVT-salts are expected to give conducting salts with electronic properties similar to those of BEDT-TTF salts.

3-7 Molecular and Crystal structures of $EOTT_2IBr_2$ and $EOTT_2AuI_2$

Fig. 12 shows the molecular structure of the EOTT molecule in the $EOTT_2IBr_2$ crystal together with the bond lengths and bond angles. The C_6S_8 portion of EOTT molecule is almost planar like EVT molecules in EVT_2PF_6 and EVT_2AsF_6. No conformational disorder was found at the ethylene group of EOTT molecule in $EOTT_2IBr_2$.

Fig. 13 shows the crystal structure of $EOTT_2IBr_2$. The IBr_2^- anion is on the center of symmetry, but 20% of IBr_2^- anions are found to be disordered. The EOTT molecules are stacked along the a-axis and the separation between the C_6S_8

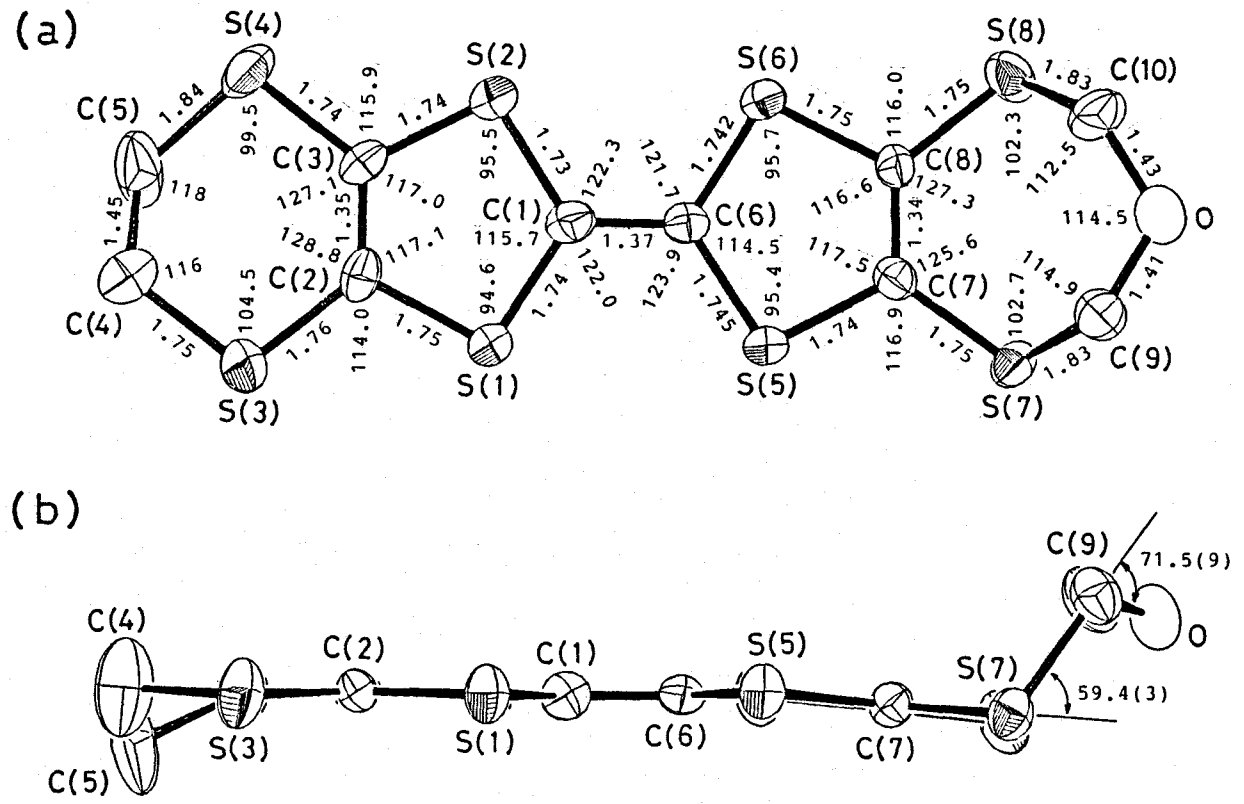

Fig. 12. Molecular structure of EOTT molecule in $EOTT_2IBr_2$.[75]
(a) Over view, (b) side view. Nonhydrogen atoms are drawn as thermal ellipsoids with 50% probability level. Estimated standard deviations of the bond lengths and bond angles are 0.009-0.03 Å and 0.5-1°, respectively.

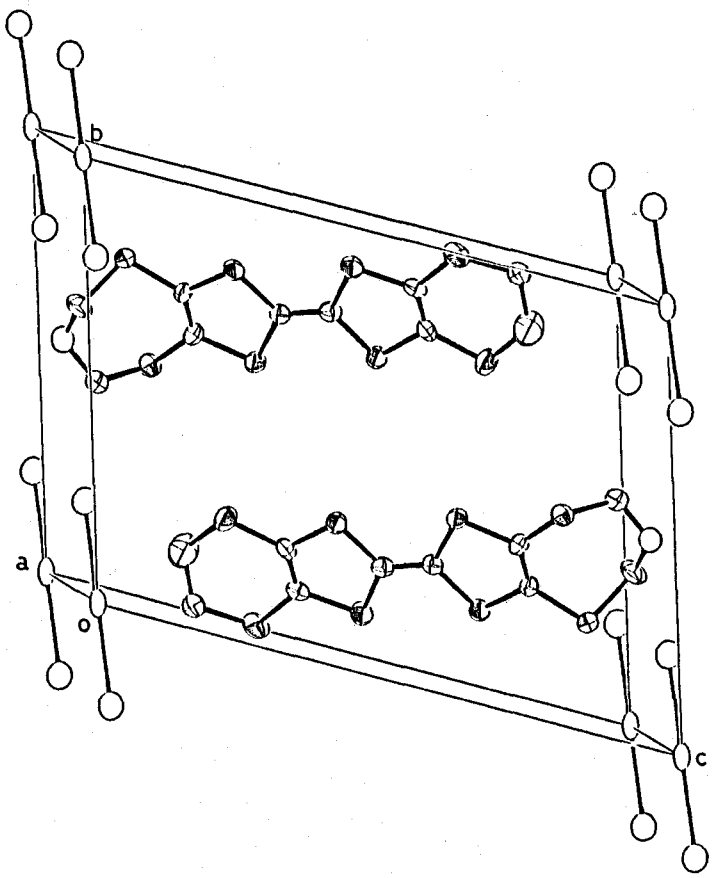

Fig. 13. Crystal structure of $EOTT_2IBr_2$.[75]

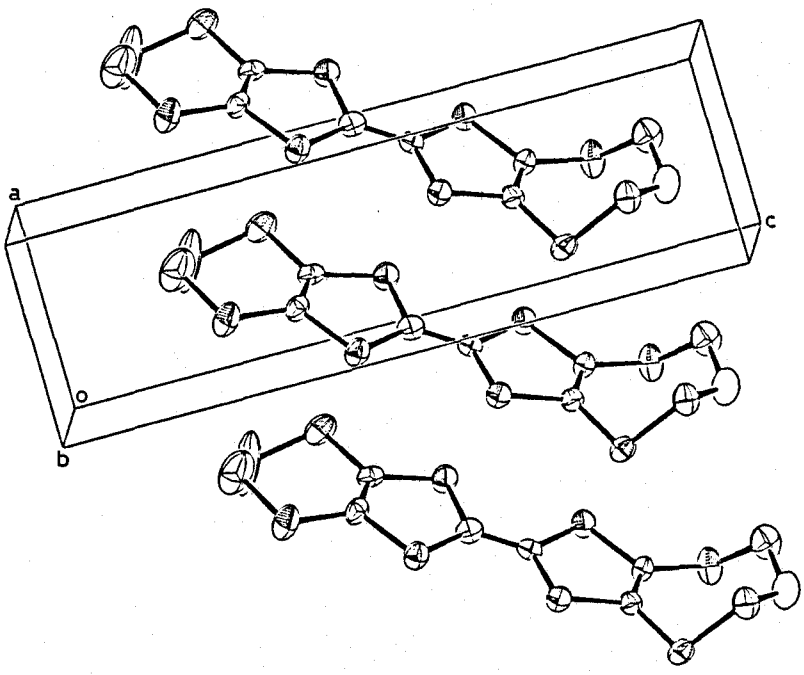

Fig. 14. Molecular arrangement within a donor column in $EOTT_2IBr_2$.

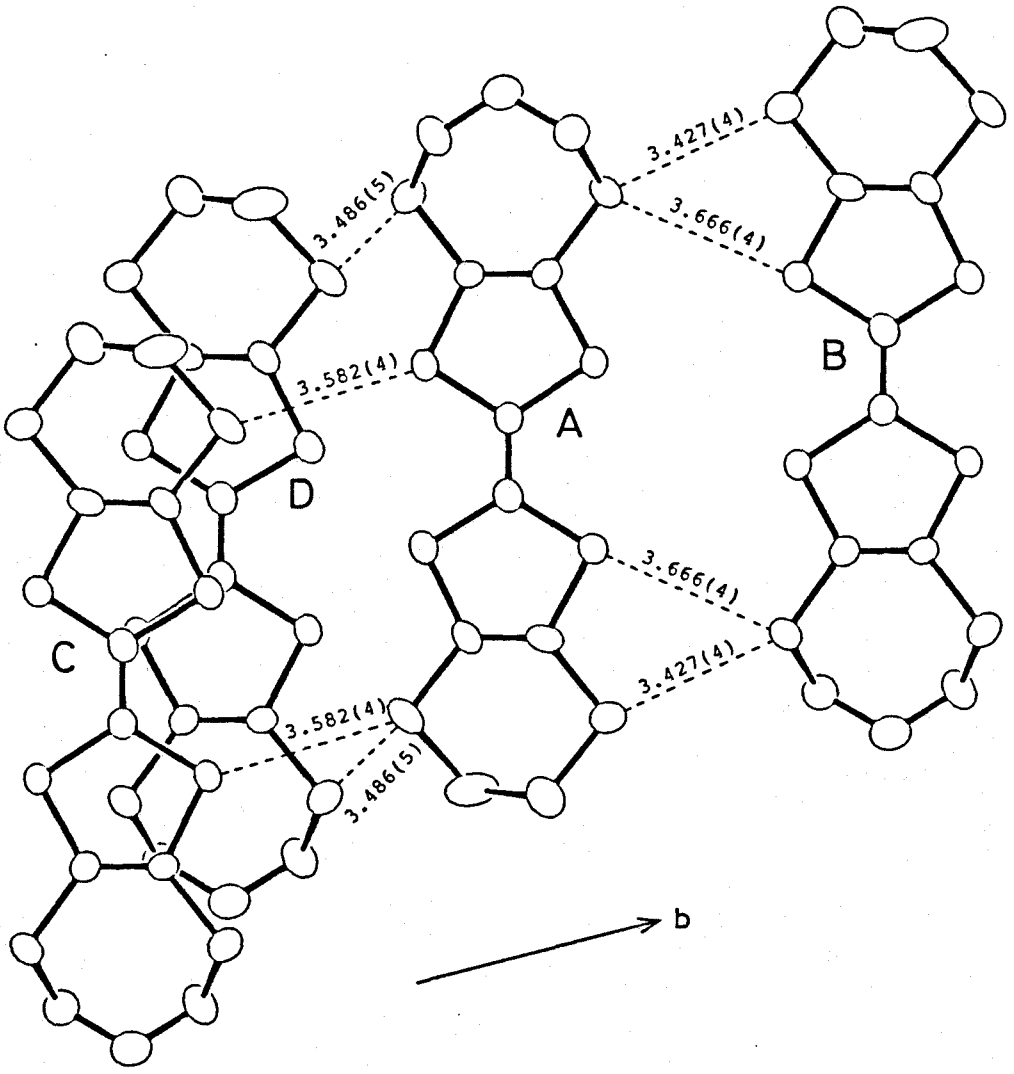

Fig. 15. Side-by-side arrangement of EOTT molecules in $EOTT_2IBr_2$. The dotted line indicates the S-S contacts shorter than the van der Waals distance (3.7 Å). Molecules A, B, C, and D correspond to those in Fig. 16.

planes in the column are identical (3.6 Å). It was noteworthy that the EOTT molecules having the unsymmetrical structure are all oriented in the same direction in a column as shown in Fig. 14. This stacking mode is different from that in EVT_2PF_6 and EVT_2AsF_6, in which the unsymmetrical donor molecules, EVT, stack alternatingly in a head-to-tail manner within a column. Only few crystal structure with the stacking mode observed for $EOTT_2IBr_2$ crystal have been reported.[54,55] Fig. 15 shows the side-by-side arrangement of EOTT molecules in $EOTT_2IBr_2$. There are many intercolumnar S-S contacts shorter than the van der Waals distance (3.7 Å) to form two-dimensional S-S networks in the crystal.

The molecular and crystal structures of $EOTT_2AuI_2$ are similar to those of $EOTT_2IBr_2$; however, the carbon atoms at the ethylene group of EOTT have very large temperature factors probably because of conformational disorder at the ethylene group.

3-8 Band Electronic Structure of $EOTT_2IBr_2$

A band electronic calculation for $EOTT_2IBr_2$ was also made based on a tight-binding method, using the molecular orbitals obtained by an extended Hückel method.

Fig. 16 and Table 22 show intermolecular overlap integrals. Since the absolute value of intracolumnar overlap integral x is much smaller than those of intercolumnar overlap integrals

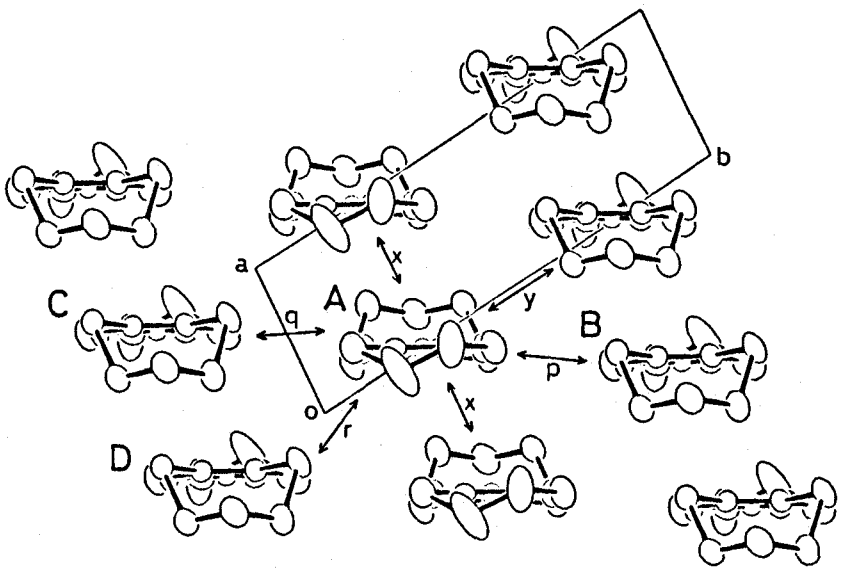

Fig. 16. Intermolecular overlap integrals (x, y, p, q, and r) of $EOTT_2IBr_2$.

Table 22.
Intermolecular Overlap Integrals of HOMO Calculated by an Extended Hückel Molecular Orbital Method

Overlap integral	$EOTT_2IBr_2$
x x 10^3	0.00
y x 10^3	7.09
p x 10^3	-1.79
q x 10^3	-1.74
r x 10^3	7.12

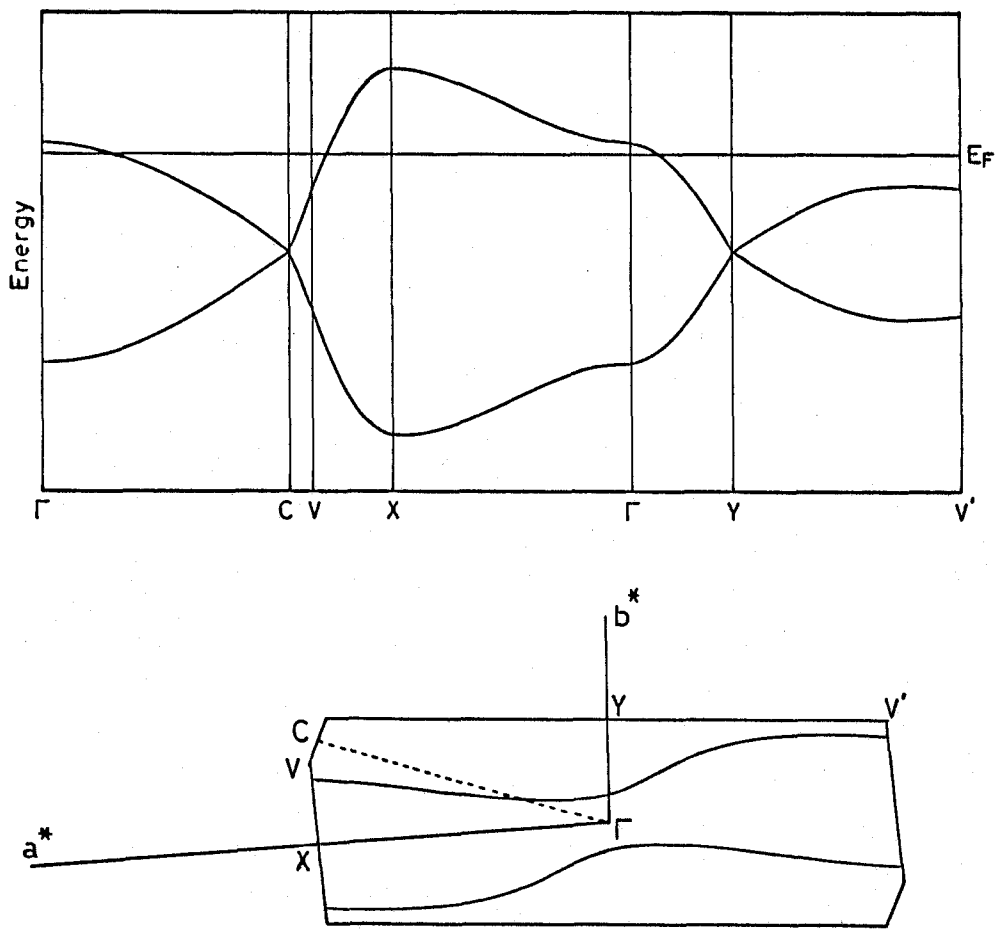

Fig. 17. Band structure and Fermi surface of $EOTT_2IBr_2$.

(y, p, q, and r), open Fermi surface with strong interaction along the b^* axis was obtained as shown in Fig. 17. However, this Fermi surface is considerably waved because of the two-dimensional nature of $EOTT_2IBr_2$.

The matrix elements (H_{ij}) of secular equation are written as follows in the case of $EOTT_2IBr_2$.

$$H_{11} = H_{22} = 2t_x \cos(ka)$$

$$H_{12} = H_{21}^* = t_y e^{-ika} + t_p e^{-i2ka} + t_q e^{-ikb} + t_r e^{-i(ka+kb)}.$$

Then, the conduction-band widths (ΔW) in the Γ-X and Γ-Y directions in Brillouin zone (see Fig. 17) are

$$\Delta W_{\Gamma-X} = 4t_x + 2(t_p + t_q)$$

and

$$\Delta W_{\Gamma-Y} = 2(t_y + t_p).$$

By adopting the overlap integrals as in the case for EVT salts, the relative conduction-band widths are 7.06 and 10.60 for $\Delta W_{\Gamma-X}$ and $\Delta W_{\Gamma-Y}$, respectively. Since the values $\Delta W_{\Gamma-X}$ and $\Delta W_{\Gamma-Y}$ are comparable, $EOTT_2IBr_2$ is assumed to have considerably two-dimensional character. This result is in accord with the fact that $EOTT_2IBr_2$ does not exhibit metal-insulator transition down to low temperature (4.2 K).

3-9 Conclusion

Molecular and crystal structures of several neutral donors and ion-radical salts have been determined. No intermolecular S-S contacts shorter than the van der Waals distance is found in

TMTVT, while there are many intermolecular S-S contacts shorter than the van der Waals distance in EVT. In the crystals of EVT_2PF_6, EVT_2AsF_6, $EOTT_2IBr_2$, and $EOTT_2AuI_2$, the columnar structures of donor molecules are formed and many intercolumnar S-S contacts shorter than the van der Waals distance are found.

Band electronic calculations have been made for EVT_2PF_6, EVT_2AsF_6, and $EOTT_2IBr_2$. The results of the calculation for EVT salts was compared with those of α-$(BEDT\text{-}TTF)_2PF_6$ and VT_2PF_6. It has been shown that the two-dimensional nature increases in the order of $VT_2PF_6 < EVT_2PF_6 < \alpha$-$(BEDT\text{-}TTF)_2PF_6$. The result of the band electronic calculation for $EOTT_2IBr_2$ shows that this ion-radical salt has considerably two-dimensional character. This result is in accord with the fact that $EOTT_2IBr_2$ exhibits metallic behavior down to 4.2 K.

General Conclusion

In the present thesis, new symmetrical and unsymmetrical TTF derivatives possessing many chalcogen atoms, their charge-transfer complexes and ion-radical salts have been synthesized, and their structures and properties investigated with the aim of exploring new highly conducting organic materials.

In chapter 1, new symmetrical and unsymmetrical TTF derivatives possessing many chalcogen atoms have been synthesized. The first half-wave oxidation potentials of the donor molecules synthesized are found to be higher than that of BEDT-TTF. The replacement of the ethylene group in BEDT-TTF by the 2-thia- or 2-oxatrimethylene group increases the on-site Coulomb repulsion energy, while the replacement by the vinylene group or the introduction of the methylthio or methylseleno group decreases the on-site Coulomb repulsion energy.

In chapter 2, charge-transfer complexes of the new donor molecules have been prepared by mixing the solutions of a donor and an acceptor. Their room-temperature conductivities are in the range from 10^{-5} to 10^{-1} S cm^{-1}. The results that the TCNQ complexes of TTT, ETTT, and TTVT exhibit fairly high conductivities ($\simeq 10^{-1}$ S cm^{-1}) are reasonably explained in terms of the amount of charge transfer as estimated from the infrared absorption spectroscopy. Ion-radical salts of new donor

molecules have been prepared by the electrochemical crystallization. Their room-temperature conductivities are in the range from 10^{-4} to 10^{2} S cm^{-1}. Some of them exhibit the metallic behavior in electrical conduction. Among them, EVT_2ReO_4, $EOTT_2IBr_2$, and $EOTT_2AuI_2$ keep metallic property down to 4.2 K.

In chapter 3, X-ray crystal structure analyses have been carried out for several neutral donors and ion-radical salts. In the crystals of EVT_2PF_6, EVT_2AsF_6, $EOTT_2IBr_2$, and $EOTT_2AuI_2$, the donor molecules are stacked to form a columnar structure and two-dimensional S-S networks are formed. Comparison of the results of band electronic calculations for EVT_2PF_6 and EVT_2AsF_6 with those for α-$(BEDT\text{-}TTF)_2PF_6$ and VT_2PF_6 shows that the two-dimensional character increases in the order of VT_2PF_6 < EVT_2PF_6 < α-$(BEDT\text{-}TTF)_2PF_6$. A band electronic calculation has also been made for $EOTT_2IBr_2$. This ion-radical salt is shown to have a two-dimensional character. This result is in accord with the fact that $EOTT_2IBr_2$ does not show any metal-insulator transition down to 4.2 K.

References

1. L. B. Coleman, M. J. Cohen, D. J. Sandman, F. G. Yamagishi, A. F. Garito, A. J. Heeger, Solid State Commun., 12, 125 (1973).
2. J. Ferraris, D. O. Cowan, V. V. Walatka Jr., J. H. Perlstein, J. Am. Chem. Soc., 95, 948 (1973).
3. D. Jerome, A. Mazand, M. Ribault, K. Bechgaard, J. Physique Lett., 41, L195 (1980).
4. E. M. Engler, CHEMTECH, 6, 274 (1976).
5. R. E. Peierls, "Quantum Chemistry of Solids", Clarendon Press: New York (1964).
6. K. Bechgaard, C. S. Jacobsen, K. Mortensen, H. J. Pedersen, N. Thorup, Solid State Commun., 33, 1119 (1980).
7. $(TMTSF)_2PF_6$: D. Jerome, A. Mazand, M. Ribault, J. Physique Lett., 41, L95 (1980).
8. $(TMTSF)_2AsF_6$: M. Ribault, G. Benedek, D. Jerome, K. Bechgaard, J. Physique Lett., 41, L397 (1980).
9. $(TMTSF)_2SbF_6$: S. S. P. Parkin, M. Ribault, D. Jerome, K. Bechgaard, J. Phys. C: Solid State Phys., 14, L445 (1981).
10. $(TMTSF)_2TaF_6$: S. S. P. Parkin, F. Crenzet, M. Ribault, D. Jerome, K. Bechgaard, J. M. Fabre, Mol. Cryst. Liq. Cryst., 79, 249 (1982).
11. $(TMTSF)_2ReO_4$: S. S. P. Parkin, D. Jerome, K. Bechgaard, Mol. Cryst. Liq. Cryst., 79, 213 (1982).

12. $(TMTSF)_2FSO_3$: R. C. Lacoe, S. A. Wolf, P. M. Chaikin, F. Wudl, E. Aharon-Shalom, Phys. Rev. B, 27, 1947 (1983).

13. $(TMTSF)_2ClO_4$: K. Bechgaard, K. Carneiro, F. B. Rasnussen M. Olsen, J. Am. Chem. Soc., 103, 2440 (1981).

14. $(BEDT\text{-}TTF)_2ReO_4$: S. S. Parkin, E. M. Engler, R. R. Schumaker, R. Lagier, V. Y. Lee, J. C. Scott, R. L. Greene, Phys. Rev. Lett., 50, 270 (1983).

15. $(BEDT\text{-}TTF)_4Hg_3Cl_8$: R. N. Lyubovskaya, R. B. Lyubovskii, R. P. Shibaeva, M. Z. Aldoshina, L. M. Gol'denberg, L. P. Rozenberg, M. L. Khidekel, Y. F. Shul'pyakov, Pis'ma Zh. Eksp. Teor. Fiz., 42, 380 (1985).

16. $(BEDT\text{-}TTF)_4Hg_3Br_8$: R. N. Lyubovskaya, E. A. Zhilyaeva, A. V. Zvarykina, V. N. Laukhin, R. B. Lyubovskii, S. I. Pesotskii, Pis'ma Zh. Eksp. Teor. Fiz., 42, 380 (1985).

17. β-$(BEDT\text{-}TTF)_2I_3$ Low Tc: K. D. Carlson, G. W. Crabtree, L. N. Hall, P. T. Copps, H. H. Wang, T. J. Emge, M. A. Beno, J. M. Williams, Mol. Cryst. Liq. Cryst., 119, 357 (1985).

18. β-$(BEDT\text{-}TTF)_2I_3$ HIGH Tc: K. Murata, M. Tokumoto, H. Anzai, H. Bando, G. Saito, K. Kajimura, T. Ishiguro, J. Phys. Soc. Jpn., 54, 1236 (1985); M. Tokumoto, K. Murata, H. Bando, H. Anzai, G. Saito, K. Kajimura, T. Ishiguro, Solid State Commun., 54, 1031 (1985).

19. θ-$(BEDT\text{-}TTF)_2I_3$: H. Kobayashi, R. Kato, A. Kobayashi, Y. Nishio, K. Kajita, W. Sasaki, Chem. Lett. 1986, 789.

20. κ-(BEDT-TTF)$_2$I$_3$: R. Kato, H. Kobayashi, A. Kobayashi, S. Moriyama, Y. Nishio, K. Kajita, W. Sasaki, Chem. Lett., 1987, 507.

21. γ-(BEDT-TTF)$_3$(I$_3$)$_{2.5}$ and α-(BEDT-TTF)$_2$I$_3$ doped with I$_2$: R. P. Shibaeva, V. F. Kaminskii, E. B. Yagubskii, Mol. Cryst. Liq. Cryst., 119, 361 (1985).

22. (BEDT-TTF)$_2$IBr$_2$: J. M. Williams, H. H. Wang, M. A. Beno, T. J. Emge, L. M. Sowa, P. T. Copps, F. Behroozi, L. N. Hall, K. D. Carlson, G. W. Crabtree, Inorg. Chem., 23, 3839 (1984).

23. (BEDT-TTF)$_2$AuI$_2$: H. H. Wang, M. A. Beno, U. Geiser, M. A. Ferestone, K. S. Webb, L. Nunez, G. W. Crabtree, K. D. Carlson, J. M. Williams, L. J. Azevedo, J. F. Kwok, J. E. Schirber, Inorg. Chem., 24, 2465 (1985).

24. (BEDT-TTF)$_3$Cl$_2$2H$_2$O: T. Mori, H. Inokuchi, Solid State Commun., 64, 335 (1987).

25. (BEDT-TTF)$_2$Cu(SCN)$_2$: H. Urayama, H. Yamochi, G. Saito, K. Oshima, A. Kawamoto, J. Tanaka, Chem. Lett., 1988, 55.

26. (BEDT-TTF)$_2$NH$_4$Hg(SCN)$_4$: H. H. Wang, K. D. Carlson, U. Geiser, W. K. Kwok, M. D. Vashon, J. E. Thompson, N. F. Larsen, G. D. McCabe, R. S. Hulscher, J. M. Williams, Physica C, 166, 57 (1990).

27. (BEDT-TTF)$_2$Ag(CN)$_2$H$_2$O: H. Mori, S. Tanaka, M. Oshima, G. Saito, K. Oshima, T. Mori, Y. Maruyama, H. Inokuchi, Synth. Met. in press.

28. $(BEDT\text{-}TTF)_2Cu[N(CN)_2]Br$: A. M. Kini, U. Geiser, H. H. Wang, K. D. Carlson, J. M. Williams, W. K. Kwok, K. G. Vandervoort, J. E. Thompson, D. L. Stupka, D. Jung, M-H. Whangbo, Inorg. Chem., 29, 2555 (1990).

29. $(BEDT\text{-}TTF)_2Cu[N(CN)_2]Cl$: H. H. Wang, M. A. Beno, K. D. Carlson, U. Geiser, A. M. Kini, J. M. Williams, Synth. Met. in press.

30. J. M. Williams, M. A. Beno, H. H. Wang, P. C. W. Leung, T. J. Emge, U. Geiser, K. D. Carlson, Acc. Chem. Res. 18, 261 (1985); J. M. Williams, K. Carneiro, Adv. Inorg. Chem. Radiochem., 29, 249 (1985).

31. A. Kobayashi, R. Kato, H. Kobayashi, S. Moriyama, Y. Nishio, K. Kajita, W. Sasaki, Chem. Lett., 1987, 459.

32. T. Suzuki, H. Yamochi, G. Srdanov, K. Hinkelmann, F. Wudl, J. Am. Chem. Soc., 111, 3108 (1989).

33. $(BEDO\text{-}TTF)_3Cu_2(NCS)_3$: M. A. Beno, H. H. Wang, A. M. Kini, K. D. Carlson, U. Geiser, W. K. Kwok, J. E. Thompson, J. M. Williams, J. Ren, M-H. Whangbo, Inorg. Chem., 29, 1599 (1990).

34. $(DMET)_2Au(CN)_2$: K. Kikuchi, M. Kikuchi, T. Namiki, K. Saito, I. Ikemoto, K. Murata, T. Ishiguro, K. Kobayashi, Chem. Lett., 1987, 931.

35. $(DMET)_2AuBr_2$ under 1.5 kbar: K. Kikuchi, K. Murata, Y. Honda, T. Namiki, K. Saito, K. Kobayashi, T. Ishiguro, I. Ikemoto, J. Phys. Soc. Jpn., 56, 2627 (1987).

36. $(DMET)_2I_3$ and $(DMET)_2IBr_2$: K. Kikuchi, K. Murata, Y. Honda, T. Namiki, K. Saito, T. Ishiguro, K. Kobayashi, I. Ikemoto, J. Phys. Soc. Jpn., 56, 3436 (1987).

37. $(DMET)_2AuCl_2$ and $(DMET)_2AuI_2$: K. Kikuchi, K. Murata, Y. Honda, T. Namiki, K. Saito, H. Anzai, K. Kobayashi, T. Ishiguro, I. Ikemoto, J. Phys. Soc. Jpn., 56, 4241 (1987).

38. $(DMET)_2AuBr_2$ under ambient pressure: K. Kikuchi, Y. Honda, Y. Ishikawa, K. Saito, I. Ikemoto, K. Murata, H. Anzai, T. Ishiguro, K. Kobayashi, Solid State Commun., 66, 405 (1988).

39. $(MDT\text{-}TTF)_2AuI_2$: G. C. Papavassiliou, G. A. Mousdis, J. S. Zambounis, A. Terzis, A. Hountas, B. Hilti, C. W. Mayer, J. Pfeiffer, Synth. Met., 27, B379 (1988).

40. R. Kato, A. Kobayashi, Y. Sasaki, H. Kobayashi, Chem. Lett., 1984 993.

41. M. Mizuno, A. F. Garito, M. P. Cava, J. Chem. Soc., Chem. Commun., 1978, 18.

42. R. Kato, H. Kobayashi, A. Kobayashi, Y. Sasaki, Chem. Lett., 1984, 1693.

43. R. Kato, H. Kobayashi, A. Kobayashi, Y. Sasaki, Chem. Lett., 1985, 1231.

44. R. Kato, H. Kobayashi, A. Kobayashi, Chem. Lett., 1986, 2013.

45. R. Kato, H. Kobayashi, A. Kobayashi, Chem. Lett., 1987, 567.

46. P. J. Nigrey, B. Morosin, J. F. Kwak, E. L. Venturini, J. E. Schirber, M. A. Beno, Synth. Met., 19, 617 (1987).

47. M. Yoshitake, K. Yakushi, H. Kuroda, A. Kobayashi, R. Kato, H. Kobayashi, Bull. Chem. Soc. Jpn., 61, 1115 (1988).
48. T. Sugano, S. Sato, M. Konno, M. Kinoshita, Synth. Met., 27, B475 (1988).
49. A. M. Kini, S. F. Tytko, J. E. Hunt, J. M. Williams, Tetrahedron Lett., 28, 4153 (1987).
50. A. M. Kini, B. D. Gates, S. F. Tytko, T. J. Allen, S. B. Kleinjan, H. H. Wang, L. K. Montgomery, M. A. Beno, J. M. Williams, Synth. Met., 27, B445 (1988).
51. G. C. Papavassiliou, G. A. Mousdis, S. Y. Yiannopouls, V. C. Kakoussis, J. S. Zambounis, Synth. Met., 27, B373 (1988).
52. G. C. Papavassiliou, V. C. Kakoussis, G. A. Mousdis, J. S. Zambounis, W. Mayer, Chem. Scripta, 29, 71 (1989).
53. A. Otsuka, G. Saito, T. Nakamura, M. Matsumoto, Y. Kawabata, K. Honda, M. Goto, M. Kurahashi, Synth. Met., 27, B575 (1988).
54. A. Otsuka, G. Saito, T. Sugano, M. Kinoshita, K. Honda, Thin Solid Films, 179, 259 (1989).
55. A. Otsuka, H. Yamochi, G. Saito, T. Sugano, M. Kinoshita, S. Sato, K. Honda, K. Ohfuchi, M. Konno, Synth. Met., in press.
56. R. Kato, H. Kobayashi, A. Kobayashi, Chem. Lett., 1989, 781.
57. T. Mori, H. Inokuchi, A. M. Kini, J. M. Williams, Chem. Lett., 1990, 1279.
58. K. Inoue, Y. Tasaka, O. Yamazaki, T. Nogami, H. Mikawa, Chem. Lett., 1986, 781.

59. T. Nakamura, S. Iwasaka, H. Nakano, K. Inoue, T. Nogami, H. Mikawa, Bull. Chem. Soc. Jpn., 66, 365 (1987).

60. T. Nogami, K. Inoue, T. Nakamura, S. Iwasaka, H. Nakano, H. Mikawa, Synth. Met., 19, 539 (1987).

61. H. Kobayashi, A. Kobayashi, T. nakamura, T. Nogami, Y. Shirota, Chem. Lett., 1987, 559.

62. S. Iwasaka, T. Nogami, Y. Shirota, Synth. Met., 26, 177 (1988).

63. G. Steimecke, H. J. Sieler, R. Kirmse, E. Hoyer, Phosphorus and Sulfur, 7, 49 (1979).

64. C. C. Price, F. V. Brutcher, J. Cohen, Org. Synth., Collective vol. 4 (1963).

65. J. S. Chappell, A. N. Bloch, W. A. Bryden, M. Maxfield, T. O. Poehler, D. O. Cowan, J. Am. Chem. Soc., 103, 2442 (1981).

66. T. Mori, A. Kobayashi, Y. Sasaki, H. Kobayashi, G. Saito, H. Inokuchi, Bull. Chem. Soc. Jpn., 57, 627 (1984).

67. P. Main, S. E. Hull, L. Lessinger, G. Germain, J-P. Declercq, and M. M. Woolfson, MULTAN 78, "A System of Computer Programs for the Automatic Solution of Crystal Structures from X-Ray Diffraction Data," Univ. of York, England and Louvain, Belgium, 1978.

68. T. Ashida, HBLS V, The Universal Crystallographic Computing System-Osaka, The Computation Center, Osaka University, 1979, p. 53.

69. "International Tables for X-Ray Crystallography," Kynoch Press, Birmingham, England, Vol. IV, (1974), p. 71.

70. W. C. Hamilton, Acta Crystallogr., 12, 609 (1959).
71. G. M. Sheldrick, SHELX-76, "Program for Crystal Structure Determination, Univ. of Cambridge, England, 1976.
72. H. Kobayashi, A. Kobayashi, Y. Sasaki, G. Saito, H. Inokuchi, Bull. Chem. Soc. Jpn., 59, 301 (1986).
73. H. Kobayashi, R. Kato, T. Mori, A. Kobayashi, W. Sasaki, G. Saito, H. Inokuchi, Chem. Lett., 1983, 759.
74. H. Kobayashi, R. Kato, A. Kobayashi, T. Mori, H. Inokuchi, Y. Nishio, K. Kajita, W. Sasaki, Synth. Met., 27, A289 (1988).
75. C. K. Johnson, ORTEP II, Report ORNL-5138, Oak Ridge National Laboratory, Tennessee, 1976.
76. W. D. S. Motherwell and W. Clegg, PLUTO 78, Program for Plotting Crystal and Molecular Structures, University of Cambridge, England, 1978.
77. Unpublished data.

List of Publication

1. Synthesis of Tetrakis(methylthio)bus(vinylenedithio)-tetrathiafulvalene (TMTVT). TTF Derivatives Possessing Twelve Sulfurs

   H. Nakano, T. Nakamura, T. Nogami, Y. Shirota,

   Chem. Lett., 1987, 1317.

2. Synthesis of Bis[1,2-bis(methylseleno)vinylenedithio]tetra-thiafulvalene (TMSVT)

   H. Nakano, T. Nogami, Y. Shirota,

   Bull. Chem. Soc. Jpn., 61, 2973 (1988).

3. The Crystal and Molecular Structures of Bis[1,2-bis-(methylthio)vinylenedithio]tetrathiafulvalene (TMTVT)

   H. Nakano, T. Nogami, Y. Shirota, S. Harada, N. Kasai,

   Bull. Chem. Soc. Jpn., 62, 2382 (1989).

4. The Synthesis of 4,5-Ethylenedithio-4',5'-vinylenedithio-tetrathiafulvalene (EVT) and Its Methyl and Dimethyl Derivatives (EMVT, EDMVT), and the Molecular and Crystal Structure of EVT.

   H. Nakano, K. Miyawaki, T. Nogami, Y. Shirota,

   S. Harada, N. Kasai,

   Bull. Chem. Soc. Jpn., 62, 2604 (1989).

5. The Crystal and Band Electronic Structures of Bis[4,5-ethylenedithio-4',5'-(vinylenedithio)tetrathiafulvalenium] Hexafluorophosphate, and Hexafluoroarsenate [EVT_2PF_6 and EVT_2AsF_6]

   H. Nakano, K. Miyawaki, T. Nogami, Y. Shirota, S. Harada, N. Kasai, A. Kobayashi, R. Kato, H. Kobayashi, Bull. Chem. Soc. Jpn., 63, 2281 (1990).

6. Synthesis of 4,5-Ethylenedithio-4',5'-(2-oxatrimethylene-dithio)tetrathiafulvalene (EOTT) and Electrical Conductivities of Their Ion-Radical Salts

   H. Nakano, K. Yamada, T. Nogami, Y. Shirota, A. Miyamoto, H. Kobayashi, Chem. Lett., 1990, 2129.

7. Synthesis of Multi-Chalcogen TTF-Derivatives and Electrical Conductivities of Their Radical-Ion Salts

   H. Nakano, S. Ikegawa, K. Miyawaki, K. Yamada, T. Nogami, Y. Shirota, Synth. Met., in press.

8. Synthesis of Bis(2-thiatrimethylenedithio)tetrathiafulvalene (TTT) and Its Unsymmetrical Analogues (ETTT, TTVT), and Electrical Conductivities of Their Charge-Transfer Complexes

   H. Nakano, S. Ikegawa, K. Miyawaki, T. Nogami, Y. Shirota, in preparation.

9. The Crystal and Band Electronic Structures of Ion-Radical Salts of 4,5-Ethylenedithio-4',5'-(2-oxatrimethylenedithio)-tetrathiafulvalene (EOTT)

H. Nakano, K. Yamada, T. Nogami, Y. Shirota, S. Harada, N. Kasai, A. Miyamoto, H. Kobayashi,

in preparation.

Acknowledgment

The work of this thesis was carried out under the guidance of Professor Yasuhiko Shirota at the Faculty of Engineering, Osaka University.

I am grateful to Professor Yasuhiko Shirota for his invaluable guidance and encouragement throughout this work.

I am also grateful to Professor Takashi Nogami of the University of Electro-Communications at present for his guidance and helpful discussion.

I would like to thank Professor Nobutami Kasai, Dr. Shigeharu Harada, and other members of Kasai laboratory for their collaboration and helpful discussion on X-ray crystallographic work.

I would like to thank to Professor Hayao Kobayashi, Dr. Akihito Miyamoto (Toho University), Dr. Akiko Kobayashi, and Dr. Reizo Kato (The University of Tokyo) for their collaboration in electrical conductivity measurement below 20 K, and for their advice and discussion on molecular orbital and band electronic calculations.

I wish to thank Dr. Naoki Noma and other members of Shirota laboratory for their encouragement and helps.

Finally, I am very thankful to my parents for their understanding and support.

H. Nakano

Hideyuki Nakano